NACA

RESEARCH MEMORANDUM

CALCULATED AERODYNAMIC LOADINGS OF M, W, AND Λ WINGS IN INCOMPRESSIBLE FLOW

By Franklin W. Diederich and W. Owen Latham

Langley Aeronautical Laboratory
Langley Field, Va.

NATIONAL ADVISORY COMMITTEE
FOR AERONAUTICS

WASHINGTON

August 30, 1951

Classification cancelled (or changed to) Unclassified

By Authority NASA Tech Pub Announcement #61
(AUTHORIZED TO CHANGE)

By 13 Apr 65

(GRADE OF OFFICER MAKING CHANGE)

11 Apr 65
DATE

NATIONAL ADVISORY COMMITTEE FOR AERONAUTICS

RESEARCH MEMORANDUM

CALCULATED AERODYNAMIC LOADINGS OF M, W, AND Λ WINGS IN INCOMPRESSIBLE FLOW

By Franklin W. Diederich and W. Owen Latham

SUMMARY

Presented are the results of theoretical incompressible-flow calculations of the spanwise lift distributions, lift-curve slopes, spanwise centers of pressure, aerodynamic centers, coefficients of damping in roll, rolling-moment coefficients due to aileron deflection, and induced-drag coefficients of twenty M, W, and Λ wings. These results are compared with similarly calculated results for ordinary swept and unswept wings.

INTRODUCTION

Interest in M, W, and Λ wings has recently increased as a result of their potentially favorable stability and aeroelastic characteristics. In order to facilitate the aerodynamic and aeroelastic appraisal of wings of this type theoretical incompressible-flow lift distributions have been calculated for twenty plan forms of the M, W, and Λ types and four angle-of-attack conditions. These lift distributions have been integrated to yield lift-curve slopes, spanwise centers of pressure, aerodynamic centers, induced drags, coefficients of damping in roll, and rolling moments due to aileron deflection. The results of these calculations are presented in this paper and compared with similar results for ordinary swept and unswept wings. The method by which the spanwise lift distributions were calculated and some of its limitations are discussed.

SYMBOLS

a.c. aerodynamic-center position (of wing, unless specified otherwise), fraction of mean aerodynamic chord rearward of leading edge of mean aerodynamic chord

A	aspect ratio $\left(b^2/S\right)$
b	wing span
c	chord, measured parallel to free stream
c_l	section lift coefficient
$\bar{c}$	average chord $\left(\frac{c_r + c_t}{2}\right)$
C_L	wing lift coefficient $\left(L/qS\right)$
C_{L_α}	wing lift-curve slope, per radian
C_l	wing rolling-moment coefficient $\left(\frac{\text{Rolling moment}}{qSb}\right)$
C_{l_d}	rolling-moment coefficient for linear antisymmetrical angle-of-attack distribution from 0 at the root to 1 radian at the tip $\left(-C_{l_p}\right)$
C_{l_p}	coefficient of damping in roll
C_{D_i}	induced-drag coefficient
d	distance of quarter-chord point of mean aerodynamic chord rearward of intersection of quarter-chord line and plane of symmetry
F	downwash factor
q	dynamic pressure
s	semispan of horseshoe vortex
S	wing area
V	free-stream velocity
w	downwash velocity
x	longitudinal ordinate
y	lateral ordinate

y^* dimensionless lateral ordinate $\left(\frac{y}{b/2}\right)$

$\bar{y}$ lateral ordinate of spanwise center of pressure

$\bar{\bar{y}}$ lateral ordinate of centroid of wing area

α_δ aileron effectiveness parameter $\left(\frac{\partial c_l}{\partial \delta}\Big/\frac{\partial c_l}{\partial \alpha}\right)$

λ taper ratio

Λ angle of sweepback at quarter-chord line

Subscripts:

B at position of spanwise discontinuity of angle of sweep

i inner

MAC pertaining to mean aerodynamic chord

o outer

r root

t tip

v made dimensionless by dividing by s

δ pertaining to a unit equivalent aileron deflection $(\alpha_\delta \delta)$

METHOD AND SCOPE OF CALCULATIONS

Basis of Method

According to two-dimensional thin-airfoil theory the lift on a section with angle of attack and parabolic camber may be calculated by locating a vortex at the quarter-chord point and setting the ratio of its induced downwash at the three-quarter-chord point to the free-stream velocity equal to the slope of the airfoil at that point. Since induction effects on unswept wings are generally in the nature of induced angles of attack and induced parabolic cambers, quite accurate lift distributions can be calculated on the basis of a bound vortex at the quarter-chord line and the slope at the three-quarter-chord line. This simple concept may be applied to swept wings as well, except that induced effects at the root are such as to invalidate the concept in

that region. Nonetheless, methods based on this concept have been used extensively for calculating lift distributions on swept wings, either with continuous distributions of vorticity over the span (reference 1) or by means of horseshoe vortices (reference 2, for instance).

In applying the same method to wings of unconventional plan form, two difficulties arise. Both of the approaches used in references 1 and 2 imply the assumption that the lift distribution can be approximated with sufficient accuracy by the first three or four terms of a Fourier series, and both of the approaches consider the downwash at only three or four points along the three-quarter-chord line. Neither of these approximations may be valid for wings with an unconventional plan form or a complicated angle-of-attack condition; however, the approximations can be avoided in part by using horseshoe vortices as in reference 2 but treating each individually rather than relating them to each other by Fourier series.

The resulting procedure is straightforward but, nonetheless, more time consuming than the methods of references 1 and 2. It has the advantage that it can be applied to plan forms and angle-of-attack distributions which cannot be treated by those methods. Also, the results of the procedure are obtained in a form which lends itself to the calculation of aeroelastic phenomena. The accuracy of the method is, for plan forms to which the methods of references 1 and 2 apply, at least as good as that of these methods. However, in applying the method to plan forms such as that of figure 1, the accuracy is affected adversely by the fact that the quarter-chord-vortex three-quarter-chord-downwash concept is not valid at the spanwise discontinuities in angle of sweep. Since this effect is local and tends to average for the entire wing, the resulting accuracy may be adequate for many purposes. As a result of these considerations, this method was used in the calculations described in this paper.

Outline of Method of Calculating Lift Distributions

The horseshoe vortices are considered to be centered on the quarter-chord line (see fig. 1), and the downwash is calculated at corresponding points on the three-quarter-chord line. In so doing, the charts and tables of the downwash due to a horseshoe vortex with unit circulation at various points relative to the vortex given in reference 3 can be used. In these charts and tables the downwash is presented in the form of a downwash factor F. The downwash angle at any point due to any horseshoe vortex may be determined by means of the equation

$$\frac{w}{V} = \frac{c_l c}{8\pi s} F \qquad (1)$$

where $c_l c$ is the loading coefficient at the station at which the horseshoe is centered, s the semispan of the horseshoe vortex, and F the factor appropriate to the relative location of the downwash point and the center of the vortex. This factor is determined by calculating the lateral and longitudinal distances, Δy and Δx, between these points and dividing them by s to get dimensionless distances Δy_v and Δx_v (in the notation of references 2 and 3), respectively; the factor corresponding to these values may then be obtained from the tables of reference 3.

The downwash angle at one point due to all vortices is obtained by performing the following summation:

$$\left(\frac{w}{V}\right)_h = \frac{\bar{c}}{8\pi s} \sum_{j=1}^{n} \left(\frac{c_l c}{\bar{c}}\right)_j F_{hj} \qquad (h = 1, 2, \ldots n) \quad (2)$$

where the subscript h designates the downwash point, j the vortex, and n the number of vortices on the total span. This addition may be shortened by setting

$$\left.\begin{aligned} \bar{F}_{hj} &= F_{hj} + F_{h,n+1-j} \\ \bar{F}_{h,\frac{n+1}{2}} &= F_{h,\frac{n+1}{2}} \end{aligned}\right\} \quad (3)$$

$$\bar{\bar{F}}_{hj} = F_{hj} - F_{h,n+1-j} \quad (4)$$

where F_{hj} is the downwash factor for a vortex on the right wing and $F_{h,n+1-j}$ the factor for the corresponding vortex on the left wing; the addition can be then confined to the right wing alone, so that

$$\left(\frac{w}{V}\right)_h = \frac{\bar{c}}{8\pi s} \sum_{j=1}^{\frac{n+1}{2}} \left(\frac{c_l c}{\bar{c}}\right)_j \bar{F}_{hj} \qquad \left(h = 1, 2, \ldots \frac{n+1}{2}\right) \quad (5)$$

or

$$\left(\frac{w}{V}\right)_h = \frac{\bar{c}}{8\pi s} \sum_{j=1}^{\frac{n-1}{2}} \left(\frac{c_l c}{\bar{c}}\right)_j \bar{\bar{F}}_{hj} \qquad \left(h = 1, 2, \ldots \frac{n-1}{2}\right) \quad (6)$$

in the symmetric and antisymmetric cases, respectively. (The upper limits in the summation apply to an odd number of vortices numbered from the right wing tip inward, with one of them, number $\frac{n+1}{2}$, on the airplane center line; if there is an even number of vortices, with the legs of two vortices coinciding with the center line, the upper limit in both equations (5) and (6) is n/2.)

Equations (5) and (6) are, in effect, simultaneous equations for $\frac{n+1}{2}$, $\frac{n-1}{2}$, or $n/2$ unknown values of $c_l c/\bar{c}$ in terms of the corresponding number of known angles of attack along the span. The values $\bar{F}_{hj}$ and $\bar{\bar{F}}_{hj}$ may be used directly as the coefficients of these equations disregarding the term $\bar{c}/8\pi s$; however, in that case the solutions of the equations must each be multiplied by the factor $8\pi s/\bar{c}$ in order to obtain the corresponding values of $c_l c/\bar{c}$. From these values the lift coefficient may be obtained by integrating the curve $c_l c/\bar{c}$ over the span.

Preliminary calculations were made with several vortex patterns, the one of reference 2 shown in figure 1, one with 20 equally spaced vortices of width equal to 0.1 of a semispan, and some with more or fewer vortices. For instance, lift distributions were calculated by means of two of these patterns and by means of the method of reference 1 for a wing of aspect ratio 4.5, taper ratio 1, with 45° sweepback. These lift distributions are shown in figure 2; the distributions and the lift-curve slopes are in excellent agreement. The possibility of using horseshoe vortices with bound parts slanted to follow the quarter-chord line more closely was also investigated.

As a result of these preliminary calculations a rectangular vortex pattern with 20 equally spaced vortices reaching from wing tip to wing tip appears to be the optimum arrangement from the point of view of computing effort commensurate with attainable accuracy. In view of the inherent limitations of the theory the increase in accuracy obtainable by resorting to a greater number of vortices or to the same number of vortices with skewed bound parts is largely spurious. The calculations of the present paper have been performed by means of this vortex representation.

The factors F were obtained from reference 4, the values of $\bar{F}$ and $\bar{\bar{F}}$ from equations (3) and (4), and the values of $c_l c/\bar{c}$ for various distributions of angle of attack or w/V by solving equation (5) for symmetrical cases and equation (6) for antisymmetrical cases. The value of s is $0.05b/2$ and hence $\bar{c}/s$ is equal to $40/A$.

Calculation of the Lift, Rolling Moment, Bending Moment, and Induced Drag

The calculated lift distributions were integrated numerically using the following factors, the lifts being those calculated by solving equations (5) and (6) and the factors being based on parabolic approximations to segments of the distributions and on the assumption that the lift distribution goes to zero with infinite slope at the wing tip:

Lift at y^* =	Calculation of -		
	Total lift	Moment (symmetrical case)	Moment (antisymmetrical case)
0.05	0.0958	0.0047	0.0044
.15	.1042	.0149	.0149
.25	.1	.0250	.0250
.35	.1	.0350	.0350
.45	.1	.0450	.0450
.55	.1	.0550	.0550
.65	.1	.0650	.0650
.75	.1	.0750	.0750
.85	.0983	.0832	.0832
.95	.0956	.0906	.0906

The induced drag was calculated in effect by obtaining the value of the lift at values of y^* equal to 0.9808, 0.9239, 0.8315, 0.7071, 0.5556, 0.3827, 0.1951, and 0 from faired curves of the spanwise lift distribution, calculating the lifting-line downwash from these values by means of the downwash factors of reference 4 (with $m = 15$ in the notation of reference 4), and integrating the products of the lifting-line downwash and the local lift by means of the integrating factors of reference 4.

Calculation of the Aerodynamic Center

Neither the method used in this paper for calculating spanwise lift distributions nor that of reference 1 furnishes any information

concerning the local centers of pressure of these lift distributions and hence the wing aerodynamic centers. The frequently made assumption that these methods imply a two-dimensional pressure distribution with a center of pressure at the quarter-chord point is not valid. In this paper the wing aerodynamic centers have been calculated on the basis of this assumption partly because the local aerodynamic centers are not known reliably and partly because the net effect of local aerodynamic centers ahead of and behind the quarter-chord line on the wing aerodynamic center may be small. In order to gain some measure of the error introduced in the wing aerodynamic center as a result of this approximation wing aerodynamic centers have also been calculated for some plan forms on the basis of assumed local aerodynamic centers based on calculations for ordinary swept and unswept wings by means of the method of reference 2.

The aerodynamic centers calculated in both ways have been expressed as fractions of the mean aerodynamic chord rearward of the leading edge of the mean aerodynamic chord. For wings with linearly varying chords, that is

$$c = c_r\left[1 - (1 - \lambda)y^*\right] \tag{7}$$

the mean aerodynamic chord is equal in size to the chord at the centroid of wing area defined by

$$\bar{\bar{y}}^* = \frac{1}{3}\frac{1 + 2\lambda}{1 + \lambda} \tag{8}$$

and, hence, is equal to

$$c_{MAC} = c_r \frac{2}{3}\frac{1 + \lambda + \lambda^2}{1 + \lambda} \tag{9}$$

The spanwise location of this chord is either in the plane of symmetry, when the wing as a whole is considered, or at the geometric centroid of wing area $\bar{\bar{y}}$, if one wing only is considered. The longitudinal location of the mean aerodynamic chord coincides with the chord at the centroid of wing area in the case of unswept and ordinary swept wings. In the case of M, W, and Λ wings the quarter-chord point of the mean aerodynamic chord is located at the distance

$$d = \bar{\bar{y}} \tan \Lambda_i\left[1 - \left(1 - \frac{\tan \Lambda_o}{\tan \Lambda_i}\right)\left(1 - y^*_B\right)^2\left(1 - \frac{1 - \lambda}{1 + 2\lambda} y^*_B\right)\right] \tag{10}$$

rearward of the intersection of the quarter-chord line and the plane of symmetry, where Λ_o and Λ_i are both positive for sweepback.

Scope of Calculations

The plan forms for which calculations have been made are listed in table I as wings 1 to 20; they include eight M wings, eight W wings, three Λ wings and one inverted Λ wing. (The suggestive designation V wing is not used for the inverted Λ wing to avoid confusion with the usage of that term in connection with ordinary swept wings.) All wings have a taper ratio of 1/2; all have angles of sweep of either zero or $\pm 45^\circ$ except wings 10 to 15, which have angles of sweep of $\pm 30^\circ$; all wings have an aspect ratio of 6 except wings 16 to 20, which have an aspect ratio of 12. Three values of the spanwise position of discontinuity in sweep, hereafter referred to as the "break," are included in this series of plan forms, namely $y^*_B = 0.3$, 0.5, and 0.7.

For all plan forms lift distributions were calculated for unit angle of attack across the span, for linear symmetrical twist from 0 at the root to unit angle of attack at the tip, for linear antisymmetric twist with unit angle of attack at the tip, and for unit effective angle of attack due to deflection of a 50-percent-span outboard aileron ($\alpha_\delta \delta = 1$). These lift distributions were integrated to obtain total lifts, rolling moments, induced drags, and wing aerodynamic centers.

For the sake of comparison lift distributions for a unit angle of attack across the span and for unit linear antisymmetric twist have also been calculated for eight ordinary swept and unswept wings, which are listed in table I as plan forms 21 to 28. The method of reference 1 was used in these calculations. Rolling-moment coefficients due to aileron deflection have not been calculated for the ordinary swept and unswept wings; they may be obtained from reference 5. However, only three points on the semispan and three terms in the series development for the lift distribution were used in the calculations of reference 5. Therefore, the results of these calculations may not be as accurate as those of this paper for wings with large values of the parameter $A/\cos \Lambda$.

RESULTS AND DISCUSSION

Spanwise Lift Distribution

The calculated spanwise lift distributions for the twenty M, W, and Λ plan forms are presented for all four unit angle-of-attack conditions considered in this paper in figures 3 to 22. The symmetrical lift distributions are plotted as $cc_l / \bar{c} C_{L_\alpha}$ against the dimensionless spanwise ordinate y^*; the antisymmetric lift distributions, as $cc_l / \bar{c} C_{l_d}$

against y^*. In order to obtain values of the loading coefficient $cc_l/\bar{c}$ for the four angle-of-attack distributions these functions must be multiplied by the values of C_{L_α} and by the value of $\left(-C_{L_p}\right)$ presented in table I, respectively.

In order to afford a comparison of the lift distributions of these wings with each other and with lift distributions of ordinary swept and unswept wings, the spanwise lift distributions for constant unit angle of attack across the span are presented also in figures 23 to 25.

Effect of sweep on spanwise lift distribution.- The lift distributions of four M and W wings of aspect ratio 6 with $y^* = 0.5$ are shown in figure 23(a) with the angle of sweep of the inner portion of the wing as a parameter. Also shown are the lift distributions of four ordinary swept wings of aspect ratio 6 with angle of sweep as a parameter. The curve labeled $\Lambda_i = -45^\circ$ pertains to plan form 2, an M wing the inner and outer parts of which are swept -45° and 45°, respectively; similarly, the curve labeled $\Lambda_i = -30^\circ$ refers to plan form 11, an M wing swept $\pm 30^\circ$, and the ones labeled $\Lambda_i = 30^\circ$ and $\Lambda_i = 45^\circ$ refer to plan forms 14 and 5, which are W wings swept ± 30 and $\pm 45^\circ$, respectively. The curve labeled $\Lambda_i = 0$ pertains to an unswept wing of aspect ratio 6, which may be considered to be the limiting case of an M or a W wing as the angle of sweep of both the inner and outer parts of the wing approaches 0.

The lift distributions of the ordinary swept wings shown in figure 23(a) exhibit the well-known characteristics of such wings. As the angle of sweep increases positively from a sweptforward to a sweptback wing the peak of the lift distribution at the root diminishes and turns into a dip; at the same time the lift near the tip increases. A similar behavior is noted for the M and W wings. The lift distribution at the roots of the wings exhibits a peak when the inner portion is swept forward and a dip when it is swept back; however, neither is as pronounced as the ones of the ordinary swept wings. The region near the break of the M and W also acts in a manner similar to that of the root of an ordinary swept wing; when the two halves of the wing are swept forward relative to the break, as in the case of a W wing, the lift distribution peaks near the break, whereas in the case of an M wing it dips at the break. Outboard of the break the M and W wings act as if they were sweptback and sweptforward wings, respectively, with their roots at the break, as may be expected, with a relatively rapid drop to zero in the case of the W wings and a relatively high level of lift near the tip in the case of the M wings.

A set of lift distributions similar to those shown for wings of aspect ratio 6 in figure 23(a) is shown in figure 23(b) for wings of aspect ratio 12; however, lift distributions are shown only for M and W

and ordinary swept wings with Λ_1 or $\Lambda = \pm 45^\circ$ and for an ordinary unswept wing. The curves are very similar to those of figure 23(a), except that for the wings with the higher aspect ratio the peaks are more pronounced and, in some cases, somewhat more localized than they are for those with the lower aspect ratio.

Effect of spanwise location of break on spanwise lift distribution.- The effect of the position of the discontinuity in sweep angle on the spanwise lift distribution is shown in figure 24. The lift distributions for plan forms 1, 2, 3 (M wings of aspect ratio 6 with sweep of $\pm 45^\circ$) as well as of plan forms 21 and 25 (ordinary swept wings of aspect ratio 6 with 45° sweepforward and sweepback, respectively) are shown in figure 24(a). The ordinary swept wings are included because they constitute the limiting cases of M wings as the position of the break approaches the tip and the root, respectively. Figure 24(a) indicates that as the position of the break moves from the root to the tip the dip associated with the break moves outboard with the break; also, a peak appears in the lift distribution at the wing root and becomes higher and less localized as the position of the break approaches the tip. Similarly, the lift distributions of W wings of aspect ratio 6 and $\pm 45^\circ$ sweepback, plan forms 4, 5, and 6, are shown in figure 24(b) along with the same ordinary swept wings as in figure 24(a). Figure 24(b) indicates that as the position of the break moves outboard the dip in the lift distribution becomes lower and generally less localized and that the peak associated with the break moves outboard with the break.

Figures 24(c) and 24(d) are similar to figures 24(a) and 24(b), except that they represent M and W wings of $\pm 30^\circ$. The limiting cases as the position of the break approaches the root or tip are plan forms 22 and 24. Although the peaks and dips of the lift distributions of figures 24(c) and 24(d) are less than those of figures 24(a) and 24(b) as a result of the smaller angles of sweep, the peaks and dips associated with the break and their movement outboard with the portion of the break are just as distinct. Figures 24(e) and 24(f) are also similar to figures 24(a) and 24(b), except that they represent wings of aspect ratio 12 so that the limiting cases as the position of the break approaches the root or tip are plan forms 26 and 28. Again, although the peaks and dips are more pronounced than those observed in figures 24(a) and 24(b), the general trends of the lift distributions are the same.

Effect of sweep of outer portion on spanwise lift distribution.- The effect on the lift distribution of the angle of sweep of the outer portion of the wing at a given angle of sweep of the inner portion of the wing is shown in figure 25. The three plan forms represented in figure 25(a) are wing 25, an ordinary sweptback wing, wing 8, a Λ wing, and wing 6, a W wing; all three plan forms have an aspect ratio of 6 and are swept back 45° in the inner 70 percent of the semispan. A comparison of the three lift distributions indicates that as the angle of sweepback

of the outer 30 percent of the wing is decreased the lift increases slightly near the tip and decreases slightly near in the inner portion of the wing, with a peak near the break. As the outer portion is swept forward the peak becomes more pronounced, the lift near the tip falls off, and the lift near the root is increased somewhat. A series of plan forms similar to those of figure 25(a) but with the position of the break at 30 percent of the semispan is represented in figure 25(b). For the plan forms represented in figure 25(b) the peak in the lift distribution becomes more pronounced, the lift at and near the root increases, and the lift near the tip decreases steadily as the outer 70 percent of the span is swept forward from a sweptback to a sweptforward position.

The series of three plan forms represented in figure 25(c) consists of an M, and inverted Λ, and an ordinary sweptforward wing of aspect ratio 6 with the inner 70 percent of the semispan swept forward 45°. Comparison of the three lift distributions indicates that as the angle of sweepforward of the outer 30 percent of the wing is decreased and then changed to sweepback the lift near the tip increases steadily, but at the break it increases at first and then decreases slightly, whereas at the root it decreases slightly at first and then increases quite rapidly.

Figure 25(d) pertains to a series of plan forms identical to that of figure 25(a), except that the wings have an aspect ratio of 12 rather than 6. The trends discussed in connection with figure 25(a) are more pronounced in the case of the series of plan forms represented in figure 25(d), but otherwise the same.

Summary of effects of various parameters on spanwise lift distribution.- As a result of these considerations of the lift distributions of M, W, and Λ wings in comparison with those of ordinary swept and unswept wings the conclusion may be drawn that the lift distributions of the M, W, and Λ plan forms exhibit the characteristics which may be expected qualitatively if they are considered to be the composites of ordinary wings; for instance, the break and the outer portion of an M wing tend to act as the root and one wing of a sweptback wing, whereas the break and the outer portion of a W wing tend to exhibit the characteristics of an ordinary sweptforward wing. The effects of the break are more pronounced for wings with larger angles of sweep than for those with smaller ones. These effects also tend to be more pronounced, although sometimes more localized, in the case of wings with relatively high aspect ratios than for wings with moderate or low aspect ratios, as may be expected from a knowledge of the lift distribution of ordinary swept wings.

Lifts, Moments, Induced Drags, and Aerodynamic Centers

The spanwise lift distributions discussed in the preceding section have been integrated to obtain lift-curve slopes, coefficients of damping in roll, spanwise centers of pressure of the additional lift distributions, induced-drag coefficients, rolling-moment coefficients due to unit equivalent aileron deflection $(\alpha_\delta \delta)$, and aerodynamic centers. The aerodynamic centers have been computed both by assuming the local aerodynamic centers to be at the quarter-chord line and the somewhat arbitrarily chosen locations shown in figure 26, which are based on the results of calculations by the method of reference 2. The results are presented in table I and figures 27 to 29 for the M, W, and Λ wings considered in this paper as well as for the comparable ordinary swept and unswept wings. The wing aerodynamic centers obtained by means of the local aerodynamic centers given in figure 26 will be referred to as the corrected aerodynamic centers and are listed as $(\text{a.c.})_{\text{corr.}}$ in table I and figures 27 to 29.

Effect of sweep on lift, drag, and aerodynamic center.- The lift-curve slopes, induced-drag ratios C_{D_i}/C_L^2, and the aerodynamic centers of M and W wings are shown plotted as functions of the angle of sweep of the inner wing portion with the position of the break as a parameter in figures 27(a) and 27(b) for wings of aspect ratios 6 and 12, respectively. The curves in figures 27(a) and 27(b) for $y^*_B = 0.5$ pertain to the series of plan forms represented in figures 23(a) and 23(b), respectively. The curves for $y^*_B = 0$ and $y^*_B = 1$ represent ordinary swept wings which constitute the limits of M and W wings as the break approaches the root or the tip. Consequently, whereas the curves for $y^*_B = 0.3$, 0.5, and 0.7 represent wings which change from an M wing to an ordinary unswept to a W wing as the angle of sweep of the inner portion of the wing increases from -45° through 0° to 45°, the curve for $y^*_B = 0$ represents an ordinary wing which varies from the 45° sweptback through the unswept to the 45° sweptforward position, and that for $y^*_B = 1$, an ordinary swept wing which changes from the 45° sweptforward to the 45° sweptback position.

The lift-curve slopes of all plan forms represented in figure 27 are highest for the unswept position and decrease as the plan forms are swept either backward or forward, either into M and W or into ordinary swept wings. The decrease in lift-curve slope is less for the true M and W wings with the breaks at 0.3, 0.5, and 0.7 of the semispan than for the ordinary swept wings or M and W wings with the breaks very near the root or tip. The induced drag of the M wings is slightly higher than

that of the ordinary swept wings, but that of the W wings with the break at 0.3 and 0.5 of the semispan is slightly lower than that of the ordinary swept wings for angles of sweep between about 10° and 35°. The aerodynamic centers are more rearward for both the swept and the M and W wings than for the unswept wing. The aerodynamic centers of the W wings are between the limits of the equivalent sweptback and sweptforward wings, but the aerodynamic centers of the M wings are farther forward than those of the equivalent ordinary swept wings. These trends are true both for the uncorrected and the corrected aerodynamic centers. Both are in good agreement with each other, within 1 or 2 percent of chord for the M and W wings and within 4 percent for the ordinary swept wings; the corrected values are generally slightly farther forward than the uncorrected ones.

For the wings of aspect ratio 12 represented in figure 27(b) the lift-curve slope decreases with sweep in almost the same manner for M and W as for ordinary swept wings. The induced drag of M wings is larger than that of the ordinary swept wing, whereas that of W wings is the same as that of the ordinary swept wing. The uncorrected aerodynamic centers (no corrected ones having been calculated) move rearward as the plan forms are swept, the change being less for the W wings than the ordinary swept wings and still less for M wings. The aerodynamic centers for y^*_B = 0.3, 0.5, and 0.7 are generally within about 0.02 chord of each other.

Effect of spanwise location of break on the lift, drag, and aerodynamic center.- Figures 28(a) and 28(b) constitute cross plots of figures 27(a) and 27(b), respectively. The aerodynamic parameters are plotted against the position of the break with the angle of sweep as a parameter. In effect, each of the series of plan forms for which lift distributions are shown in figure 24 is represented by a curve (for each of the aerodynamic parameters) in figure 28. The curves of figure 28 serve to corroborate the conclusion reached in examining figure 27 that the effect of the position of the break is relatively small on both the lift-curve slope and on the induced-drag coefficient; in the case of the wings with taper ratio 0.5 considered in this paper the least induced drag is incurred for W wings with angle of sweep between 0° and 30° and the position of the break between 0.2 and 0.6 of the semispan. Except for the M wing with 45° of sweep the aerodynamic center moves generally forward as the position of the break is moved outboard from the root to the tip.

Effect of sweep of outer portion on the lift, drag, and aerodynamic center.- The effect on the aerodynamic coefficients of changes in the angle of sweep of the outer wing portion while maintaining that of the inner wing portion at a given value is shown in figure 29, which represents series of plan forms similar to those represented in figure 25. If the position of the break, which is the parameter of the

curves of figure 29, is at the root, the entire wing is swept in these series; if the position is at the tip, the plan form is unchanged and is, in the case of figures 29(a) and 29(c), a 45° sweptback wing and in the case of figures 29(b) and 29(d), a 45° sweptforward wing. If the position of the break is at 0.3, 0.5, or 0.7 of the semispan the plan form, in the case of figures 29(a) and 29(c), changes from a W to a Λ to an ordinary sweptback wing as the angle of sweepback of the outer panel is increased from -45° through 0° to 45°; in the case of figures 29(b) and 29(d) the plan form changes from an ordinary sweptforward to an inverted Λ to an M wing as the angle of sweepback is increased from -45° to 45°.

Figure 29(a) shows that as the angle of sweepback of the outer portion is increased from -45° to 45° the lift-curve slope first increases then decreases, with a maximum near the true Λ-wing condition of an unswept outer wing portion. This maximum is higher when more of the wing portion is involved in this sweeping process, that is, the closer the position of the break is to the wing root. The induced drag is a minimum for the ordinary swept wing represented by $y^*_B = 0$ between 0° and 10° of sweepforward. For $y^*_B = 0.5$ and 0.7 the induced drag is highest near the Λ-wing condition and less for either the W-wing or ordinary sweptback-wing condition; for $y^*_B = 0.3$ the drag appears to be substantially independent of the angle of sweep of the outer panel. The aerodynamic centers of the plan forms with $y^*_B = 0.3$ and 0.5 are between those with $y^*_B = 0$ and $y^*_B = 1.0$; the curve for $y^*_B = 0.7$, however, is on the side of the curve for $y^*_B = 1.0$ away from that for $y^*_B = 0$. For values of $y^*_B = 0$, 0.3, and 0.5 the aerodynamic center is most forward for the Λ-wing condition, for $y^*_B = 0.7$ it is most rearward for this condition, and for $y^*_B = 1.0$ it is constant, since the plan form is the same for all values of the ordinate, Λ_o. As noted in connection with figure 27(a) the corrected and uncorrected aerodynamic-center values are generally within 0.02 chord of each other, the corrected ones being slightly more forward on the average.

For the wings represented in figure 29(b) with the inner portion swept forward 45°, the lift-curve slope has a maximum when the outer portion is unswept (the inverted Λ-wing condition), the maximum value being higher the farther the break is inboard. The induced-drag curves have minima between 0° and 15° sweepforward of the outer portion, the drag being the lower the more of the wing is swept back, that is, the farther the break is inboard. The aerodynamic centers move forward as the outer panel is swept back from -45° to 45° of sweepback, except that if the entire wing is swept, that is, if $y^*_B = 0$, the aerodynamic center moves rearward for positive values of Λ_o. The corrected aerodynamic centers are generally within about 0.03 chord of the uncorrected ones and slightly farther forward on the average.

Figures 29(c) and 29(d) are similar to figures 29(a) and 29(b) but pertain to wings of aspect ratio 12. The trends of the curves of the aerodynamic coefficients as functions of the angle of sweepback of the outer wing portion are very similar to those shown in figures 29(a) and 29(b).

Limitations of the Results

The lift distributions calculated in this paper as well as the other aerodynamic parameters obtained by integrating the lift distributions are subject to certain limitations in consequence of the approximations made in the calculations. These approximations may be considered to be of two types, those in the manner in which a true lifting-surface (thin-wing, potential-flow) solution is effected by the method of calculation used in this paper, and those in the degree to which a thin-wing potential-flow solution represents reality.

The quarter-chord-vortex three-quarter-chord-downwash concept is known to be capable of furnishing generally excellent results for the spanwise lift distribution, although it furnishes no information whatever concerning the local centers of pressure of lift distribution. This concept fails near the root of swept wings, since in this region the chordwise pressure distribution cannot be approximated by a superposition of two-dimensional angle-of-attack-type and parabolic-camber-type pressure distributions. For ordinary swept wings this shortcoming is not serious, and its effects, which appear to be small, can be localized by using many points along the span in methods of the type of those of references 1 and 2 or by considering each vortex individually as in the present paper. For an M, W, or Λ wing, however, the effects of this shortcoming of the one-quarter-chord-vortex three-quarter-chord-downwash concept are somewhat more serious, because it affects the regions near the break as well as near the root.

Another limitation on the results calculated in this paper is imposed by the deviation of potential theory from actuality. On swept wings the boundary layer tends to flow along the span and accumulate in the downstream regions of the wing, that is, the tip of a sweptback wing and the root of a sweptforward wing. This accumulation causes a decrease in the lift in the affected region. Consequently, sweptforward wings do not always exhibit the peak in the lift distribution predicted by theory, nor do sweptback wings carry as high a level of lift near their tips. The same phenomenon must be expected on M and W wings. Consequently, the magnitude of the peak in the lift distribution at the break of a W wing may be reduced and, in some conditions, changed into a dip. Similarly, the M wing is likely to carry less lift near its root and tip than predicted by theory as a result of boundary-layer effects. These changes in the spanwise lift distribution are likely to be reflected

in a lower lift-curve slope, a more forward aerodynamic center than given in this paper, and an induced drag which may be either somewhat larger or somewhat smaller than that predicted on the basis of the calculations of this paper, depending on the nature of the change in the lift distribution.

Inasmuch as the theoretically computed results are qualitatively in line with the ones that might be expected from experience with ordinary swept wings, there is a possibility that a knowledge of the effects of the boundary layer on the aerodynamic characteristics of ordinary swept wings may serve to correct the results presented in this paper for such effects. Another possibility is that the accumulation of the boundary layer may be controlled, by means of suitable fences, for instance, in which case the results presented in this paper would be more nearly applicable.

The calculation of the aerodynamic centers in this paper is open to question on the grounds that the local aerodynamic centers are not known, those presented in figure 26 being in the nature of carefully considered estimates only. However, comparison of the wing aerodynamic centers calculated on the basis of these values with those calculated on the assumption of local aerodynamic centers at the quarter chord are in good agreement, those calculated by means of the estimated aerodynamic centers being only slightly farther forward on the average. Consequently, the aerodynamic centers are probably as accurate as the other aerodynamic parameters presented in this paper.

Compressibility effects have not been taken into account in the calculations of the lift distributions and the other aerodynamic parameters. With angles of sweep between 30° and 45° compressibility effects are not likely to be important up to free-stream Mach numbers of about 0.6 or 0.7. At higher free-stream Mach numbers the three-dimensional Glauert-Prandtl correction may serve to correct the results presented in this paper for compressibility effects in an approximate manner. At Mach numbers higher than 0.8 or 0.9, however, the corrected results are likely to possess only limited utility.

CONCLUDING REMARKS

The results of theoretical incompressible-flow calculations of the spanwise lift distributions, lift-curve slopes, spanwise centers of pressure, aerodynamic center, coefficient of damping in roll, and rolling-moment coefficient due to aileron deflection of twenty M, W, and Λ plan forms have been presented and compared with similarly calculated results for ordinary swept and unswept wings. The aerodynamic characteristics of M, W, and Λ wings are, qualitatively, those that

would be expected on the basis of knowledge of the characteristics of ordinary swept wings. The theoretically calculated induced drags of these wings differ little from those of ordinary swept wings.

Langley Aeronautical Laboratory
National Advisory Committee for Aeronautics
Langley Field, Va.

REFERENCES

1. Weissinger, J.: The Lift Distribution of Swept-Back Wings. NACA TM 1120, 1947.

2. Falkner, V. M.: The Calculation of Aerodynamic Loading on Surfaces of any Shape. R. & M. No. 1910, British A.R.C., 1943.

3. Diederich, Franklin W.: Charts and Tables for Use in Calculations of Downwash of Wings of Arbitrary Plan Form. NACA TN 2353, 1951.

4. Multhopp, H.: Die Berechnung der Auftriebsverteilung von Tragflügeln. Luftfahrtforschung, Bd. 15, Lfg. 4, April 6, 1938, pp. 153-169. (Available as R.T.P. Translation No. 2392, British M.A.P.)

5. De Young, John: Theoretical Antisymmetric Span Loading for Wings of Arbitrary Plan Form at Subsonic Speeds. NACA TN 2140, 1950.

TABLE I.- SUMMARY OF GEOMETRIC AND AERODYNAMIC PARAMETERS

Wing	Geometric parameters							Aerodynamic parameters						
	Plan form	Type	A	λ	Λ_1 (deg)	Λ_o (deg)	y^*_B	C_{l_α}	C_{D_i}/C_L^2	$-C_{l_p}$	$\bar{y}^*$	a.c.	$(a.c.)_{corr.}$	C_{l_β}
1		M	6	1/2	-45	45	0.3	3.63	0.0578	0.370	0.441	0.250	0.263	0.401
2		M	6	1/2	-45	45	.5	3.54	.0587	.379	.430	.262	.257	.422
3		M	6	1/2	-45	45	.7	3.46	.0586	.378	.416	.304	.288	.433
4		W	6	1/2	45	-45	.3	3.55	.0553	.359	.406	.343	.325	.401
5		W	6	1/2	45	-45	.5	3.57	.0549	.368	.429	.312	.294	.402
6		W	6	1/2	45	-45	.7	3.57	.0549	.378	.450	.275	.270	.409
7		Λ	6	1/2	45	0	.3	4.16	.0549	.440	.448	.255	.244	.488
8		Λ	6	1/2	45	0	.7	3.69	.0574	.408	.466	.315	.319	.446
9		Inv. Λ	6	1/2	-45	0	.7	3.55	.0564	.400	.418	.297	.276	.456
10	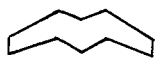	M	6	1/2	-30	30	.3	4.11	.0563	.414	.440	.244		.454
11		M	6	1/2	-30	30	.5	3.97	.0571	.413	.430	.250		.461
12	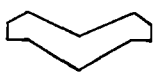	M	6	1/2	-30	30	.7	4.00	.0559	.415	422	.258		.467
13	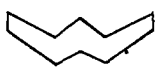	W	6	1/2	30	-30	.3	4.08	.0532	.408	.418	.289		.455
14	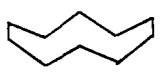	W	6	1/2	30	-30	.5	4.12	.0532	.415	.431	.277		.457

TABLE I.- SUMMARY OF GEOMETRIC AND AERODYNAMIC PARAMETERS - Concluded

Wing	Geometric paremeters							Aerodynamic parameters						
	Plan form	Type	A	λ	Λ_1 (deg)	Λ_o (deg)	y^*_B	C_{l_α}	C_{D_i}/C_L^2	$-C_{l_p}$	$\bar{y}^*$	a.c.	$(a.c.)_{corr.}$	C_{l_β}
15	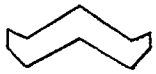	W	6	1/2	30	-30	.7	4.13	.0543	.421	.444	.260		.459
16		M	12	1/2	-45	45	.3	3.91	.0350	.472	.450	.322		.480
17		M	12	1/2	-45	45	.5	3.85	.0358	.477	.438	.326		.537
18		W	12	1/2	45	-45	.5	4.02	.0294	.491	.448	.408		.536
19		W	12	1/2	45	-45	.7	3.87	.0295	.483	.464	.411		.521
20		Λ	12	1/2	45	0	.7	4.07	.0318	.530	483	.277		.578
21		Swept	6	1/2	-45	-45		3.33	.0575	.342	.378	.418	.374	
22		Swept	6	1/2	-30	-30		3.91	.0546	.388	.401	.318		
23	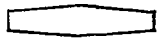	Unswept	6	1/2	0	0		4.32	.0530	.413	.425	.250	.239	
24	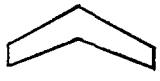	Swept	6	1/2	30	30		3.98	.0540	.390	.444	.255		
25		Swept	6	1/2	45	45		3.44	.0556	.355	.455	.294	.310	
26		Swept	12	1/2	-45	-45		3.87	.0304	.469	.341	.700		
27	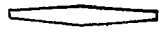	Unswept	12	1/2	0	0		5.16	.0276	.555	.429	.250		
28	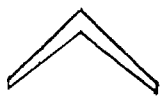	Swept	12	1/2	45	45		3.94	.0299	.457	.476	.470		

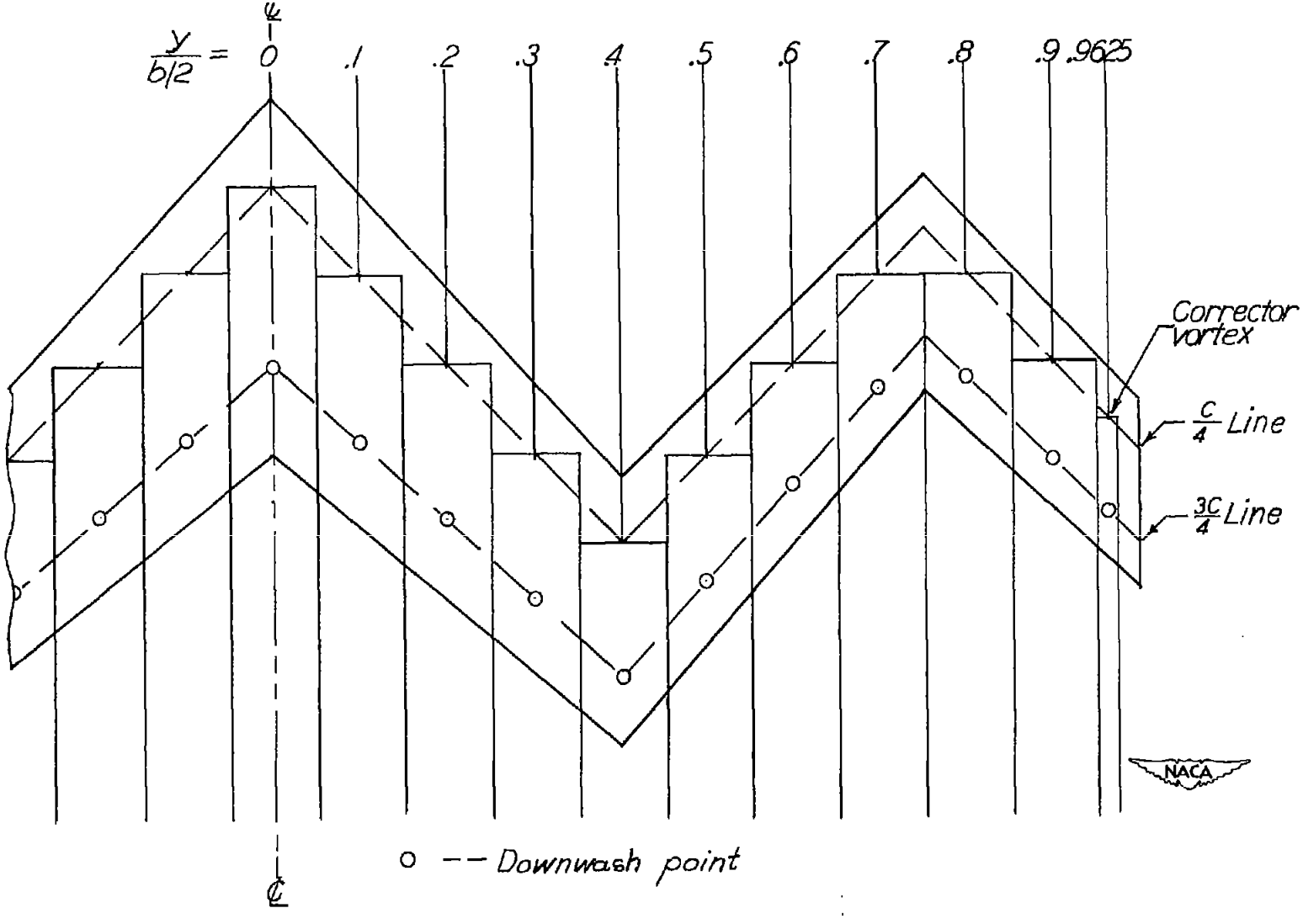

Figure 1.- Location of horseshoe vortices and downwash points on an arbitrary plan form.

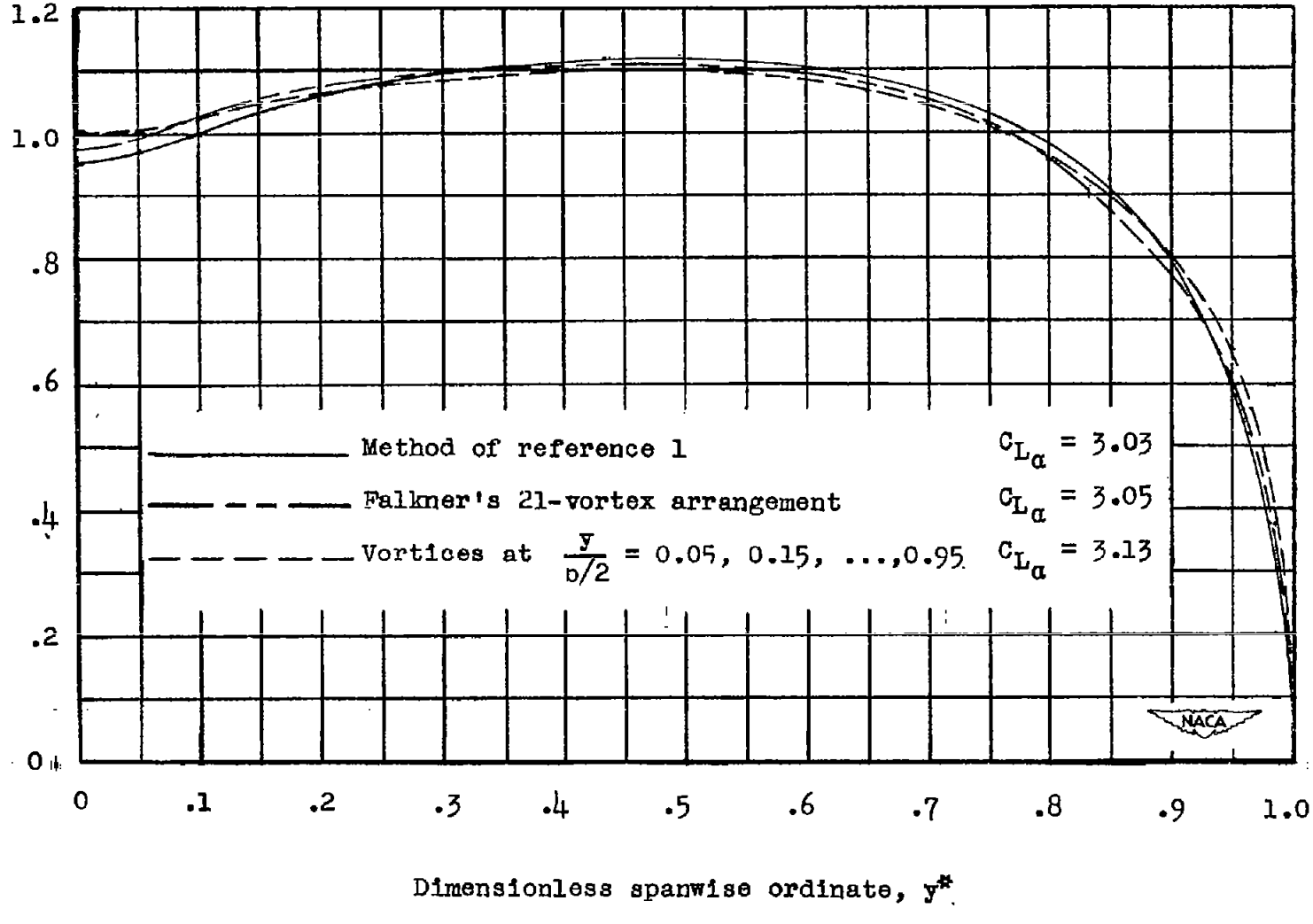

Figure 2.- Lift distributions calculated by three methods for wing with aspect ratio 4.5, taper ratio 1, sweepback = 45°.

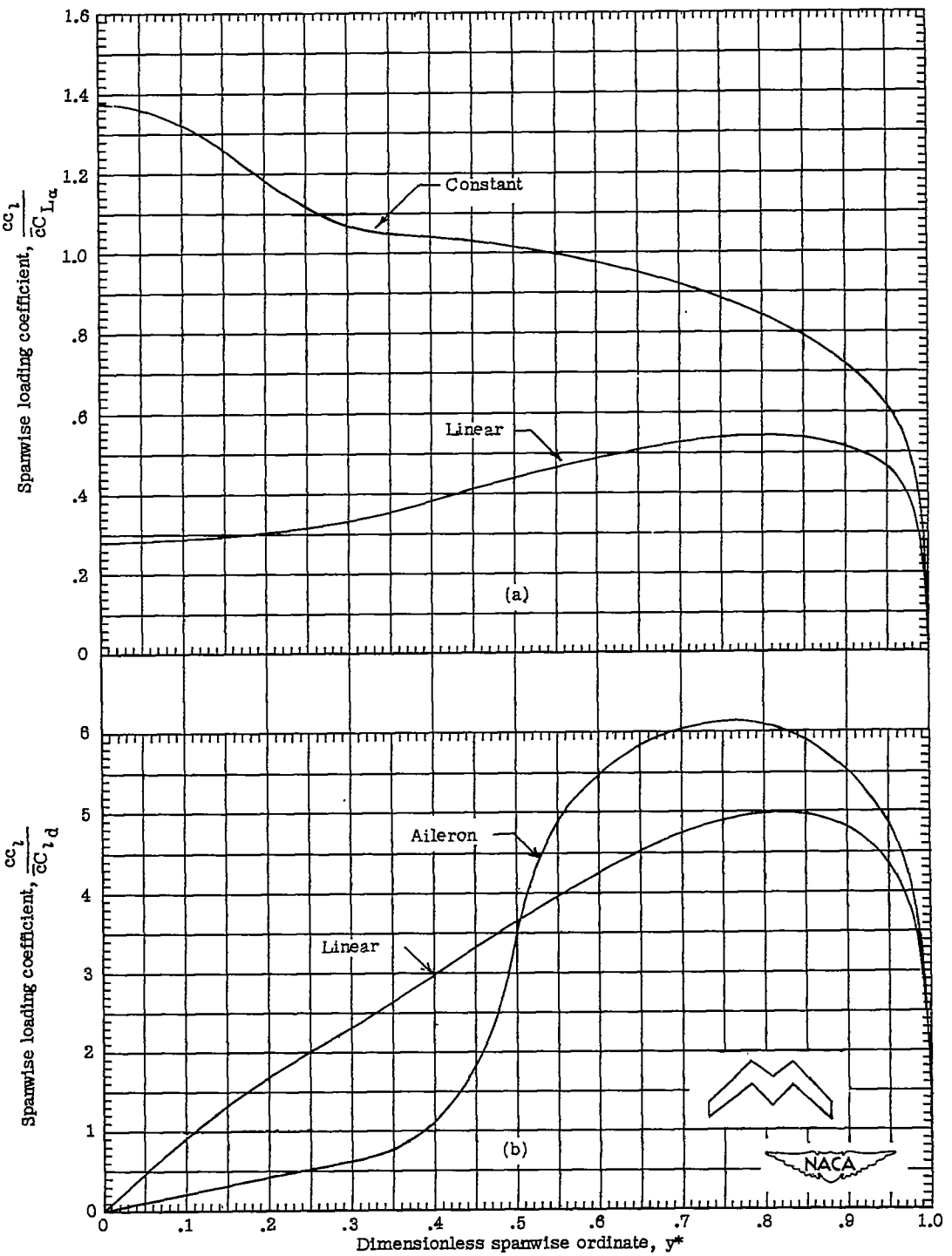

(a) Symmetrical lift distributions.

(b) Antisymmetrical lift distributions.

Figure 3.- Spanwise lift distributions for plan form 1 (A = 6, λ = 0.5, $\Lambda = \pm 45^\circ$, M wing, $y_B^* = 0.3$).

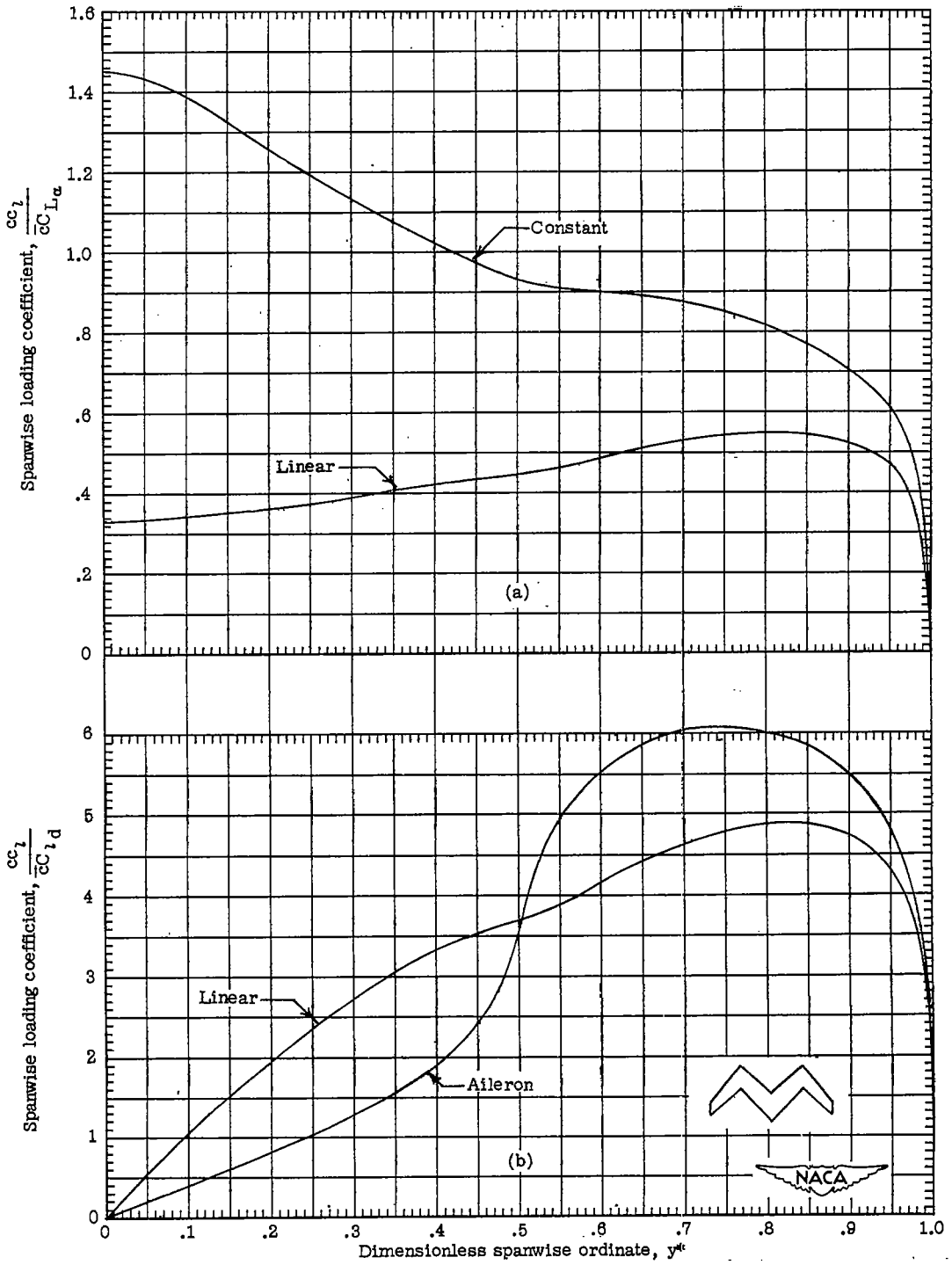

(a) Symmetrical lift distributions.

(b) Antisymmetrical lift distributions.

Figure 4.- Spanwise lift distributions for plan form 2 (A = 6, λ = 0.5, $\Lambda = \pm 45^\circ$, M wing, $y_B^* = 0.5$).

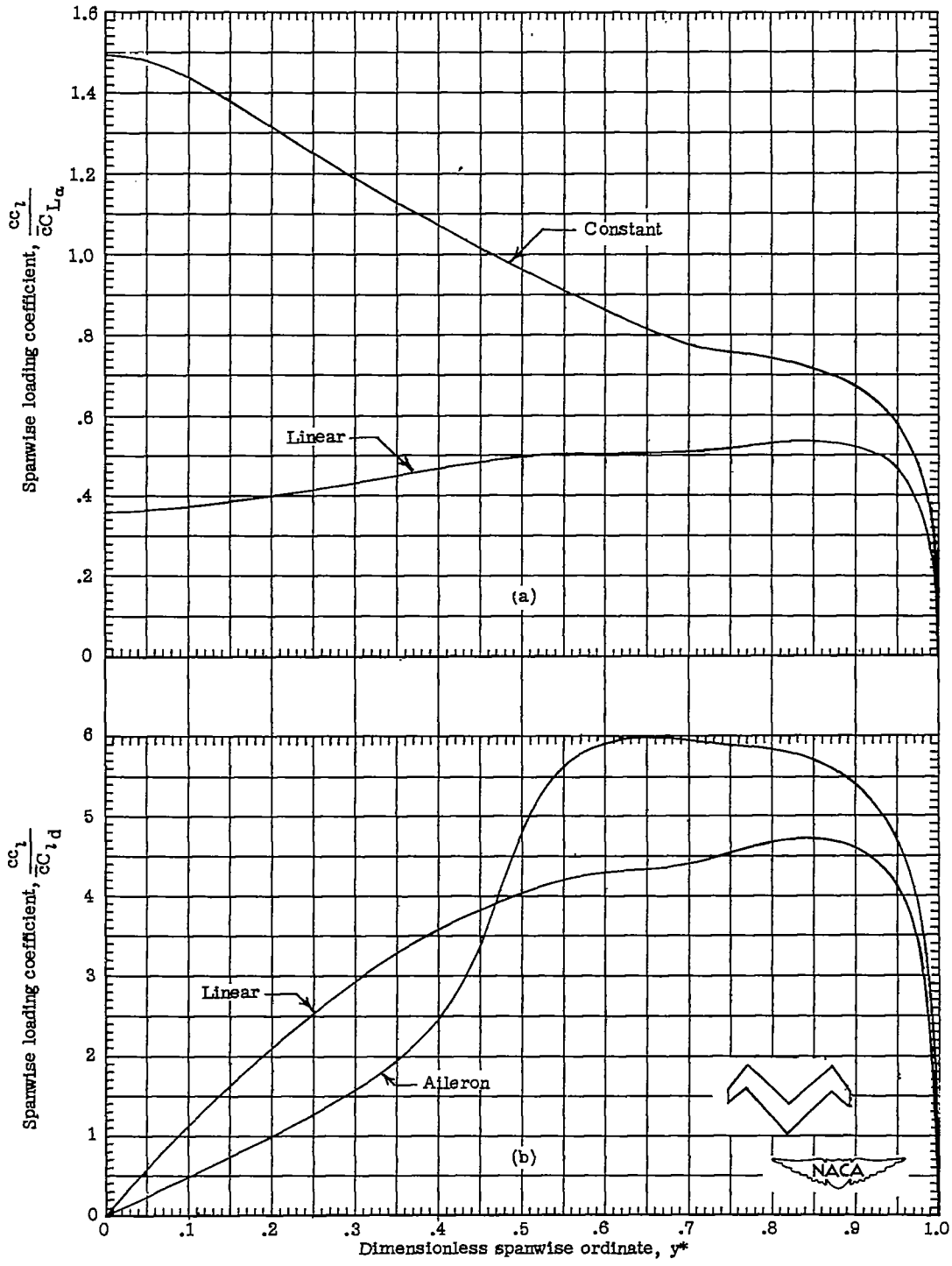

(a) Symmetrical lift distributions.

(b) Antisymmetrical lift distributions.

Figure 5.- Spanwise lift distributions for plan form 3 (A = 6, λ = 0.5, $\Lambda = \pm 45^\circ$, M wing, $y_B^* = 0.7$).

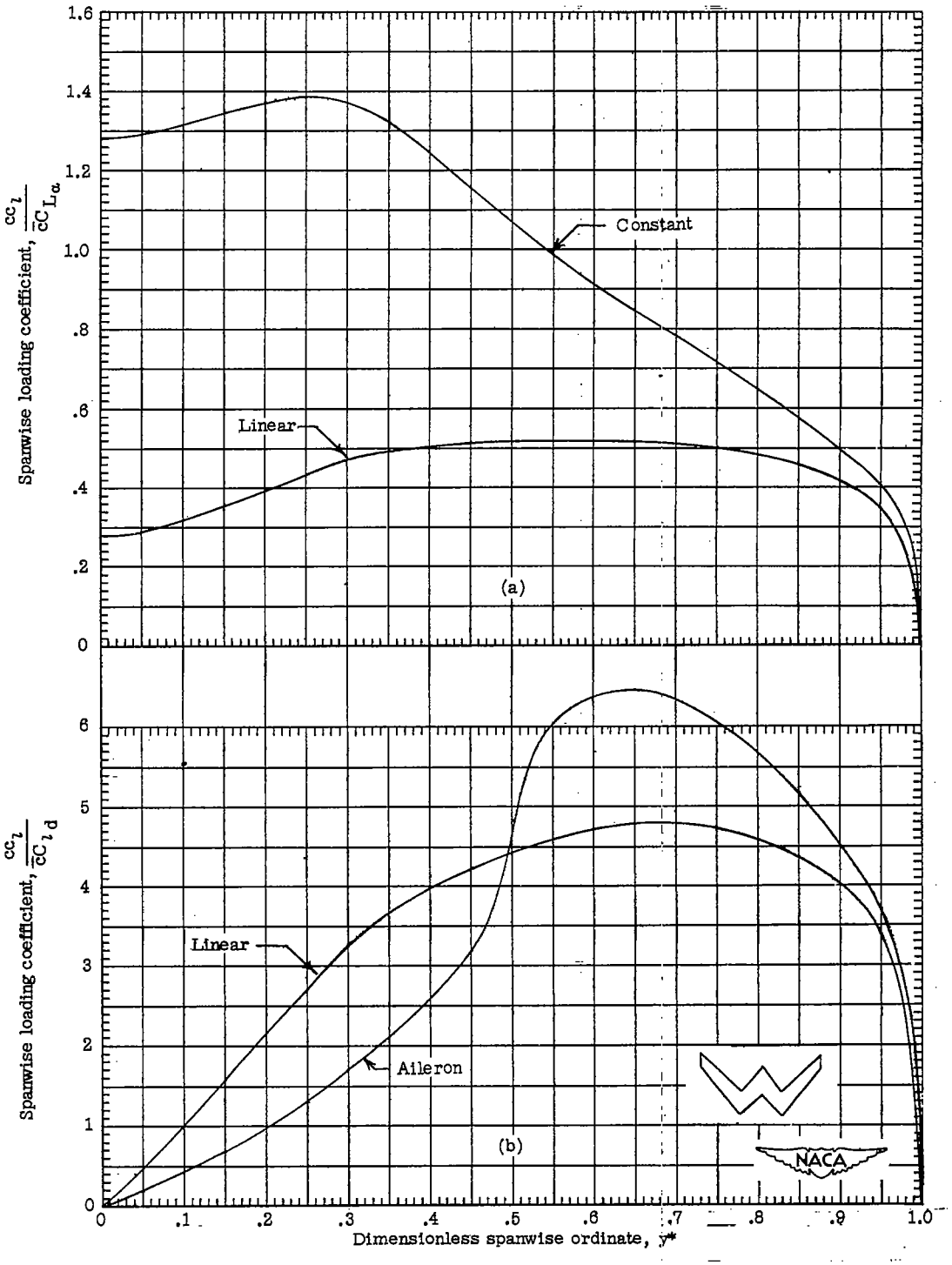

(a) Symmetrical lift distributions.

(b) Antisymmetrical lift distributions.

Figure 6.- Spanwise lift distributions for plan form 4 (A = 6, λ = 0.5, Λ = ±45°, W wing, y_B^* = 0.3).

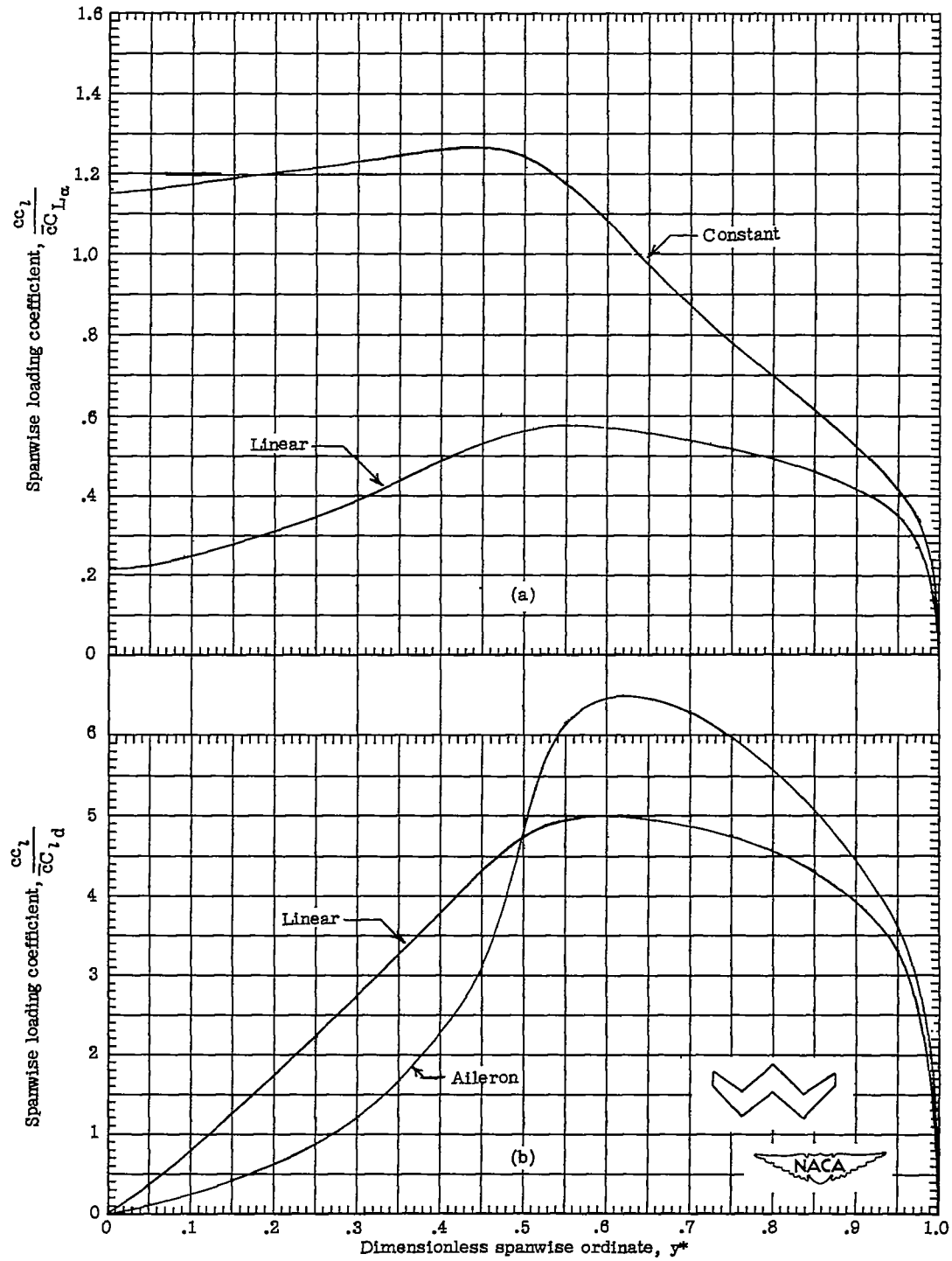

(a) Symmetrical lift distributions.

(b) Antisymmetrical lift distributions.

Figure 7.- Spanwise lift distributions for plan form 5 (A = 6, λ = 0.5, $\Lambda = \pm 45^\circ$, W wing, $y_B^* = 0.5$).

[redacted]

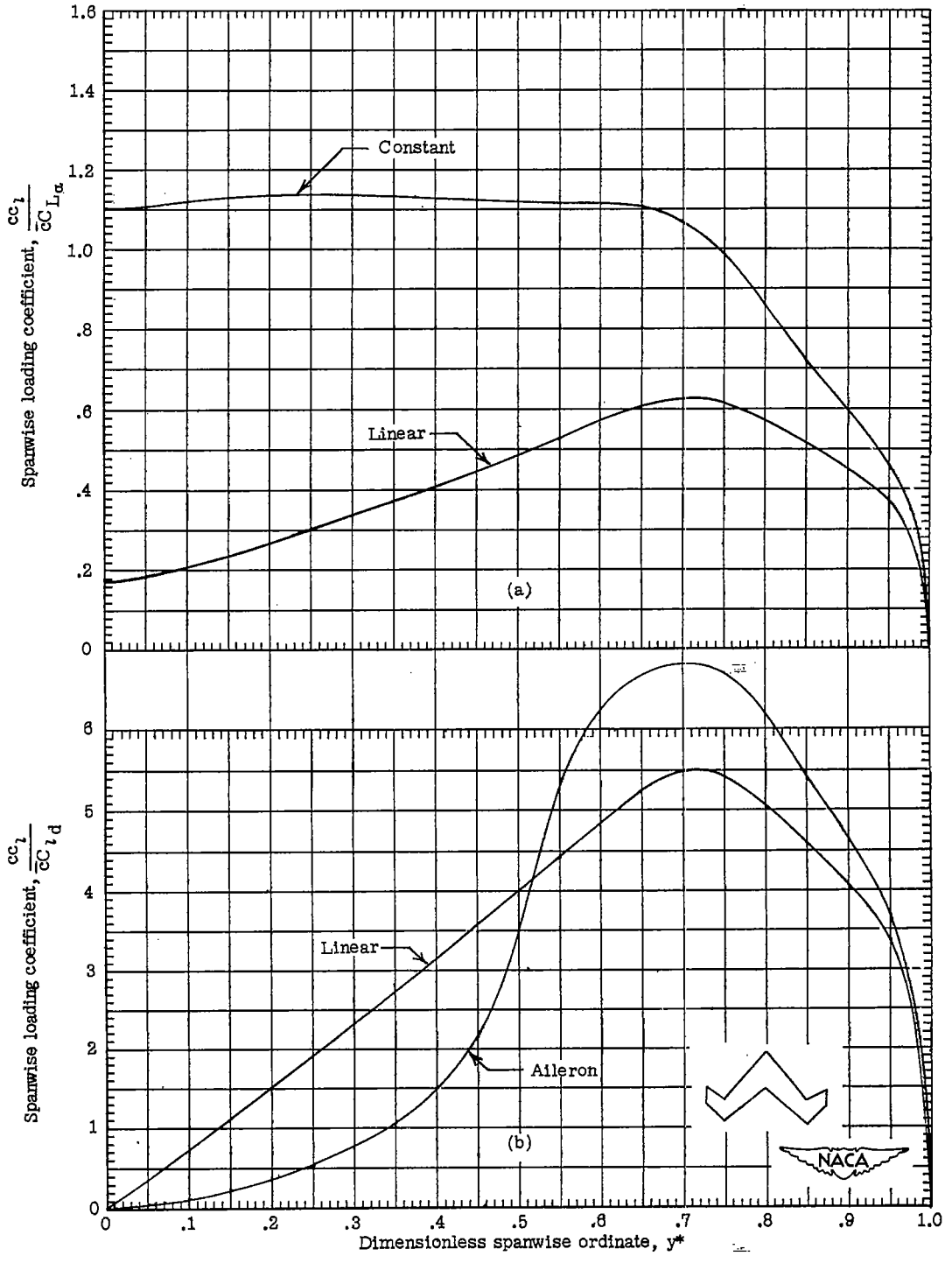

(a) Symmetrical lift distributions.

(b) Antisymmetrical lift distributions.

Figure 8.- Spanwise lift distributions for plan form 6 (A = 6, λ = 0.5, $\Lambda = \pm 45^\circ$, W wing, $y_B^* = 0.7$).

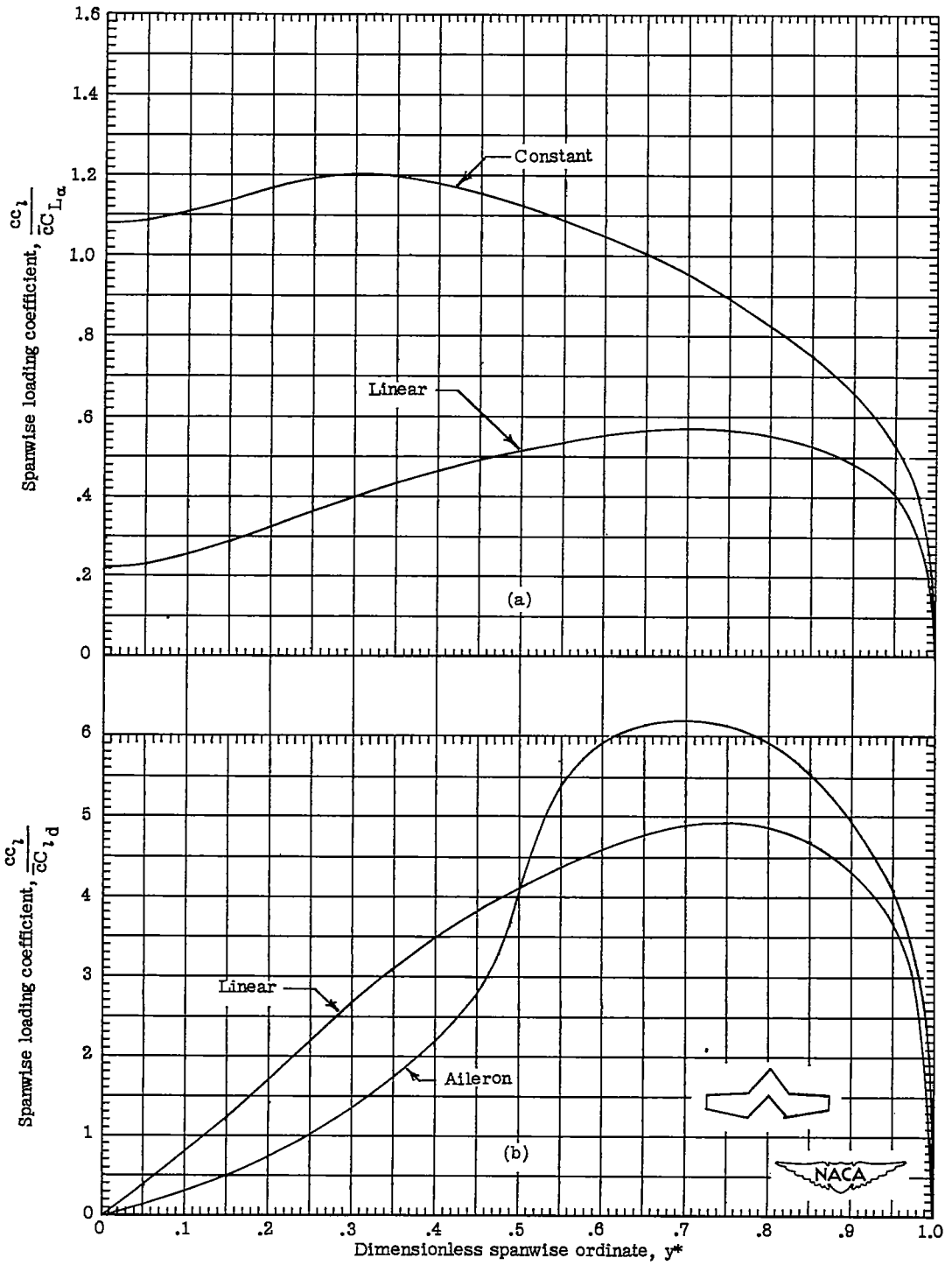

(a) Symmetrical lift distributions.

(b) Antisymmetrical lift distributions.

Figure 9.- Spanwise lift distributions for plan form 7 (A = 6, λ = 0.5, $\Lambda_i = 45^\circ$, Λ wing, $y_B^* = 0.3$).

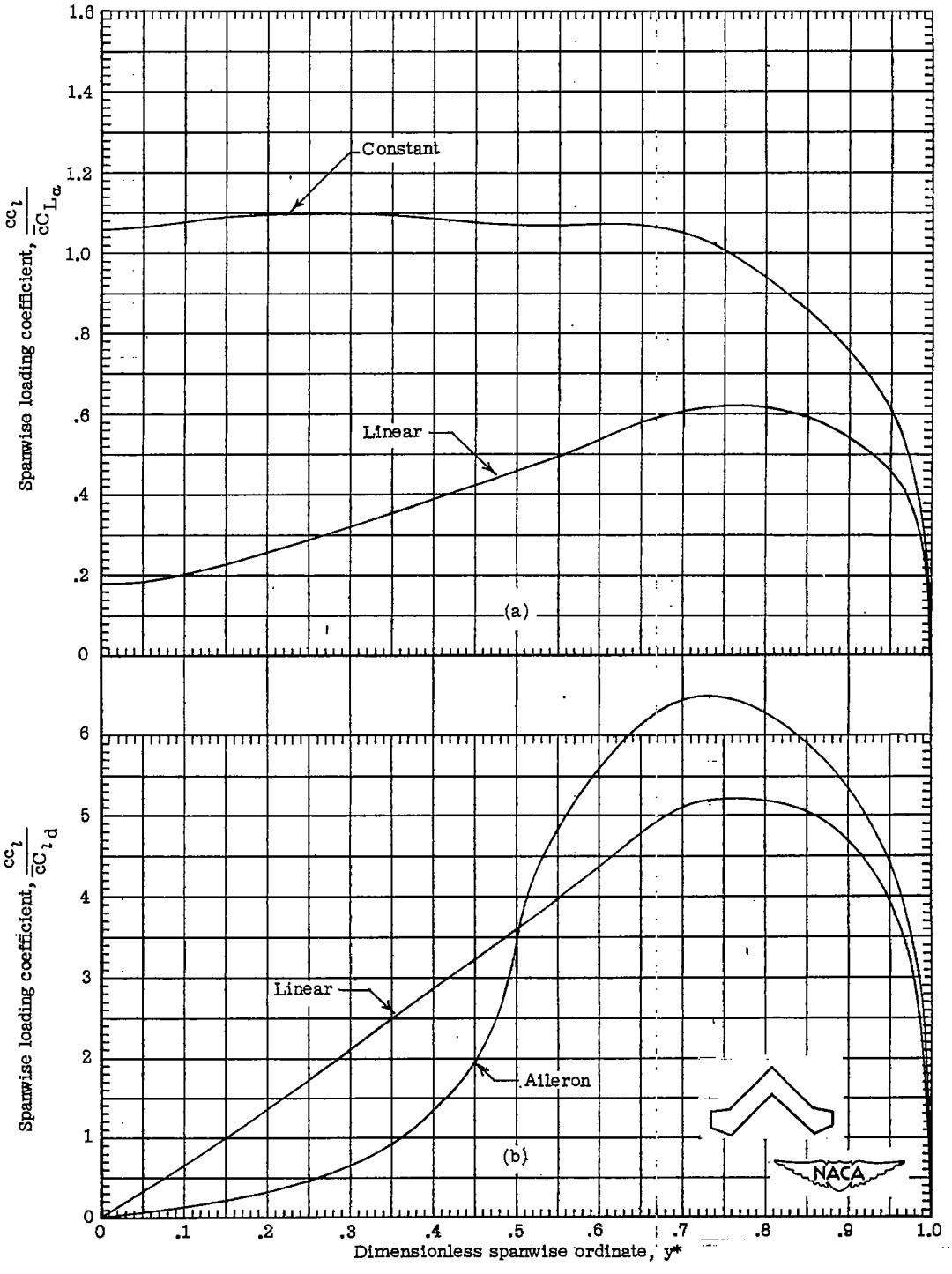

(a) Symmetrical lift distributions.

(b) Antisymmetrical lift distributions.

Figure 10.- Spanwise lift distributions for plan form 8 (A = 6, λ = 0.5, Λ_1 = 45°, Λ wing, y_B^* = 0.7).

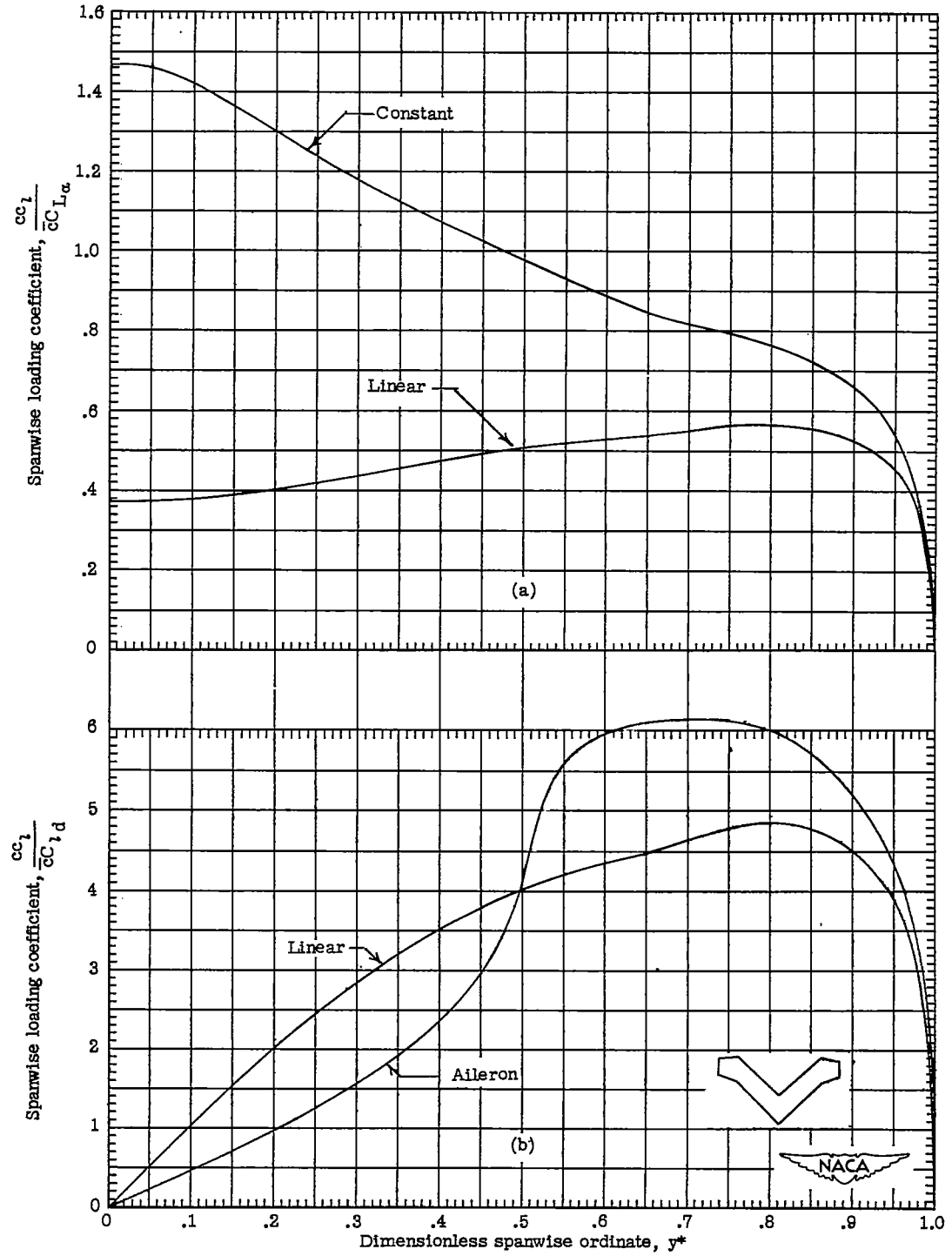

(a) Symmetrical lift distributions.

(b) Antisymmetrical lift distributions.

Figure 11.- Spanwise lift distributions for plan form 9 (A = 6, λ = 0.5, Λ_l = -45°, inverted Λ wing, y_B^* = 0.7).

[redacted]

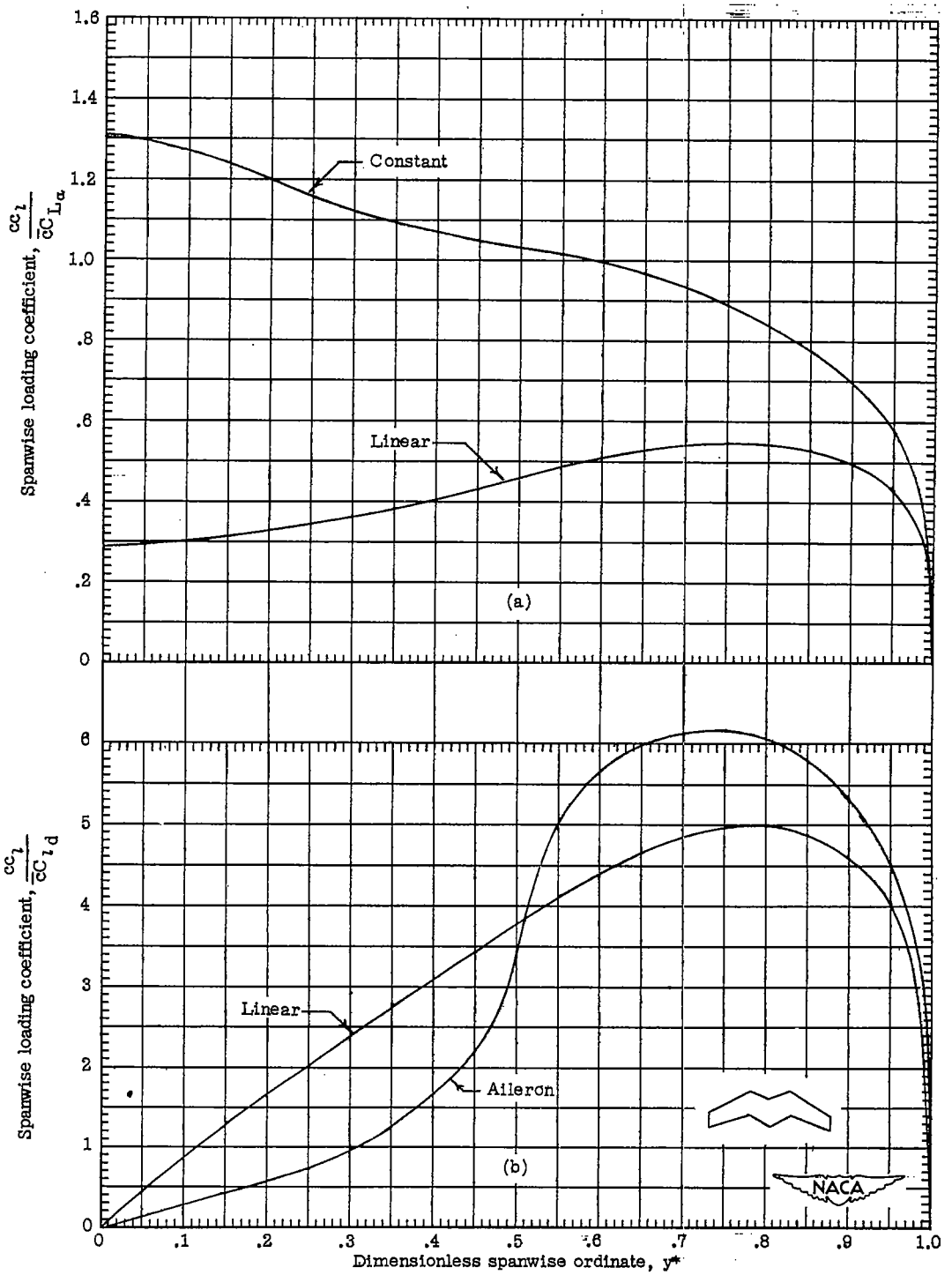

(a) Symmetrical lift distributions.

(b) Antisymmetrical lift distributions.

Figure 12.- Spanwise lift distributions for plan form 10 (A = 6, λ = 0.5, Λ = ±30°, M wing, y_B^* = 0.3).

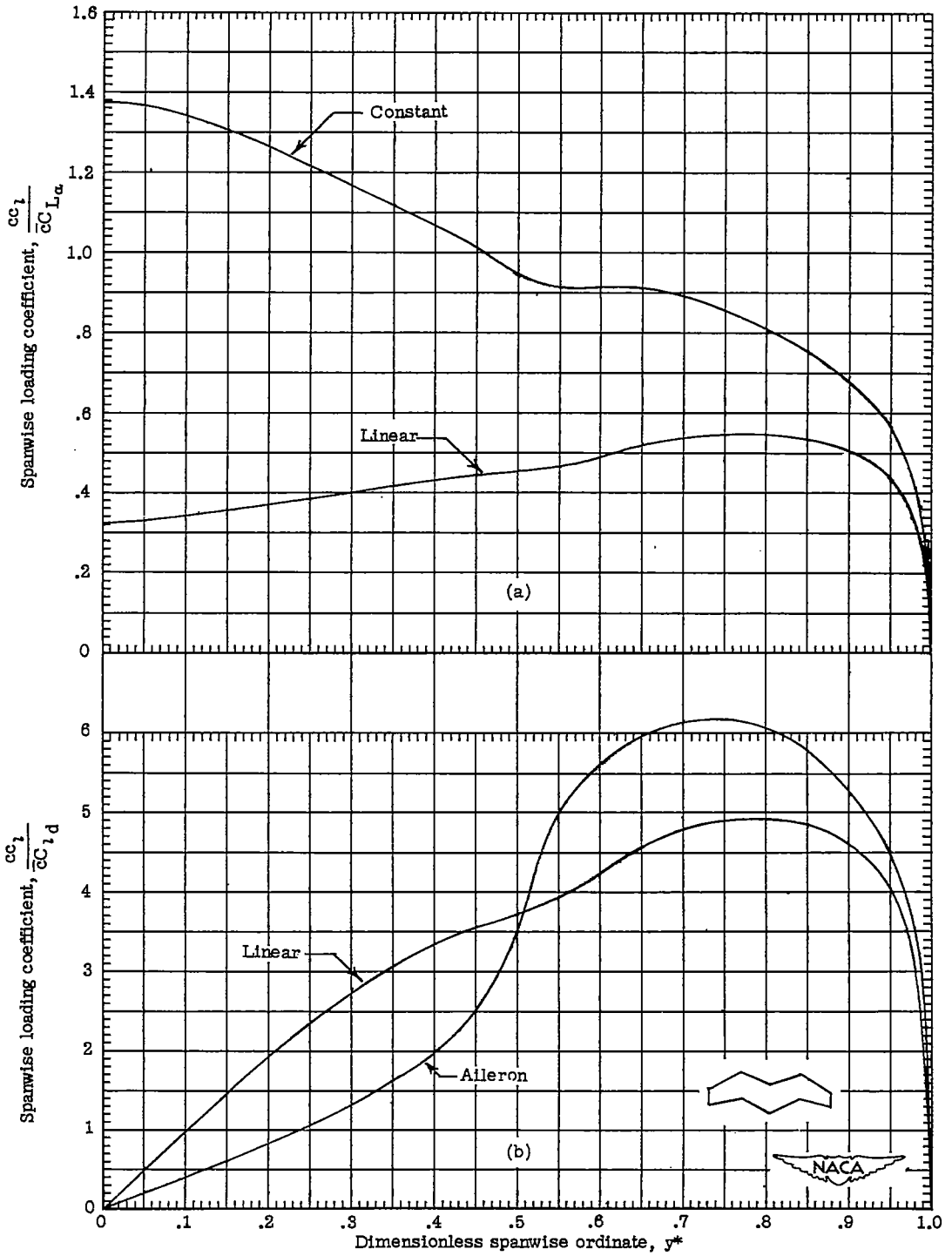

(a) Symmetrical lift distributions.

(b) Antisymmetrical lift distributions.

Figure 13.- Spanwise lift distributions for plan form 11 (A = 6, λ = 0.5, $\Lambda = \pm 30^\circ$, M wing, $y_B^* = 0.5$).

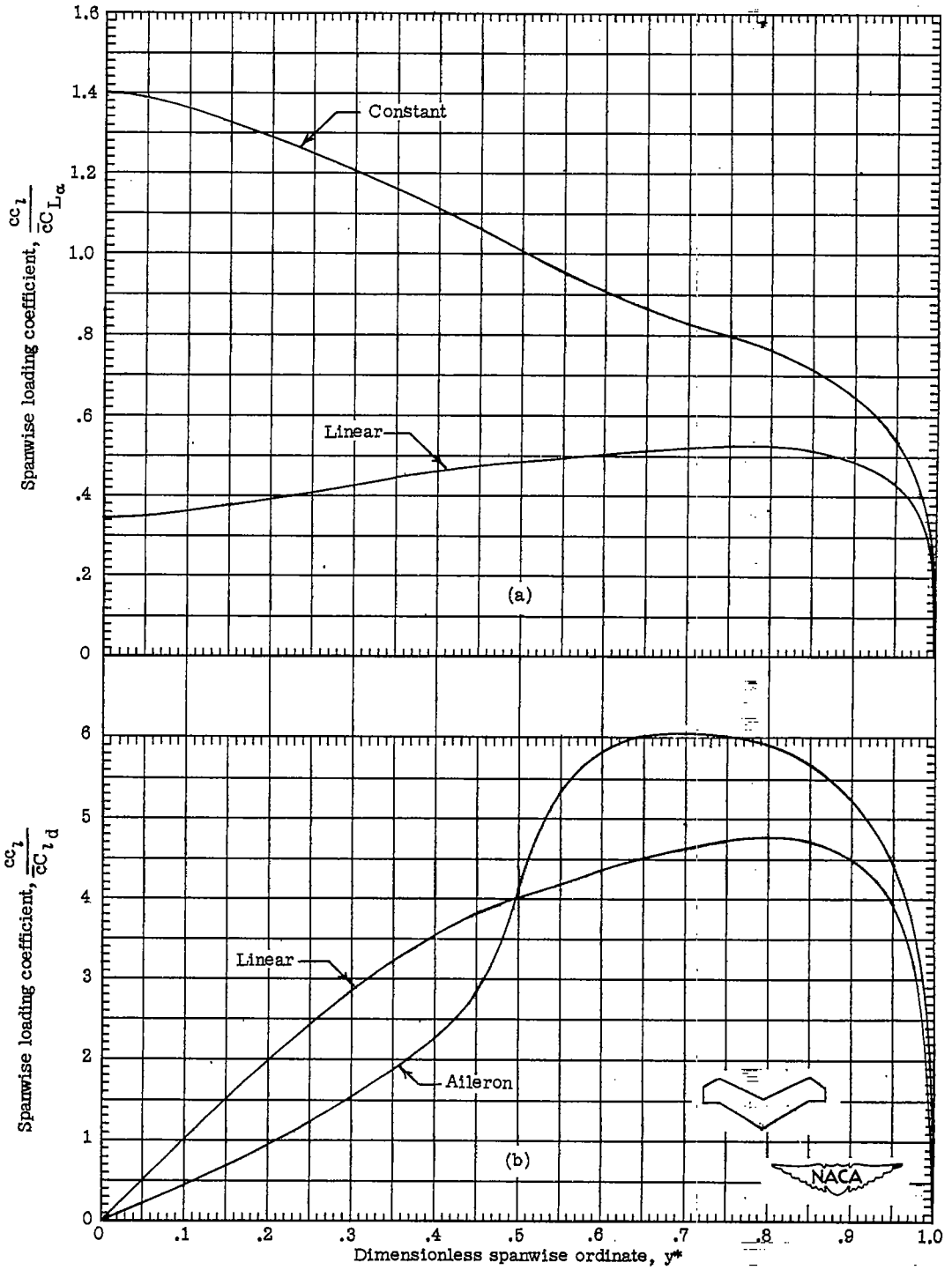

(a) Symmetrical lift distributions.

(b) Antisymmetrical lift distributions.

Figure 14.- Spanwise lift distributions for plan form 12 (A = 6, λ = 0.5, $\Lambda = \pm 30^\circ$, M wing, $y_B^* = 0.7$).

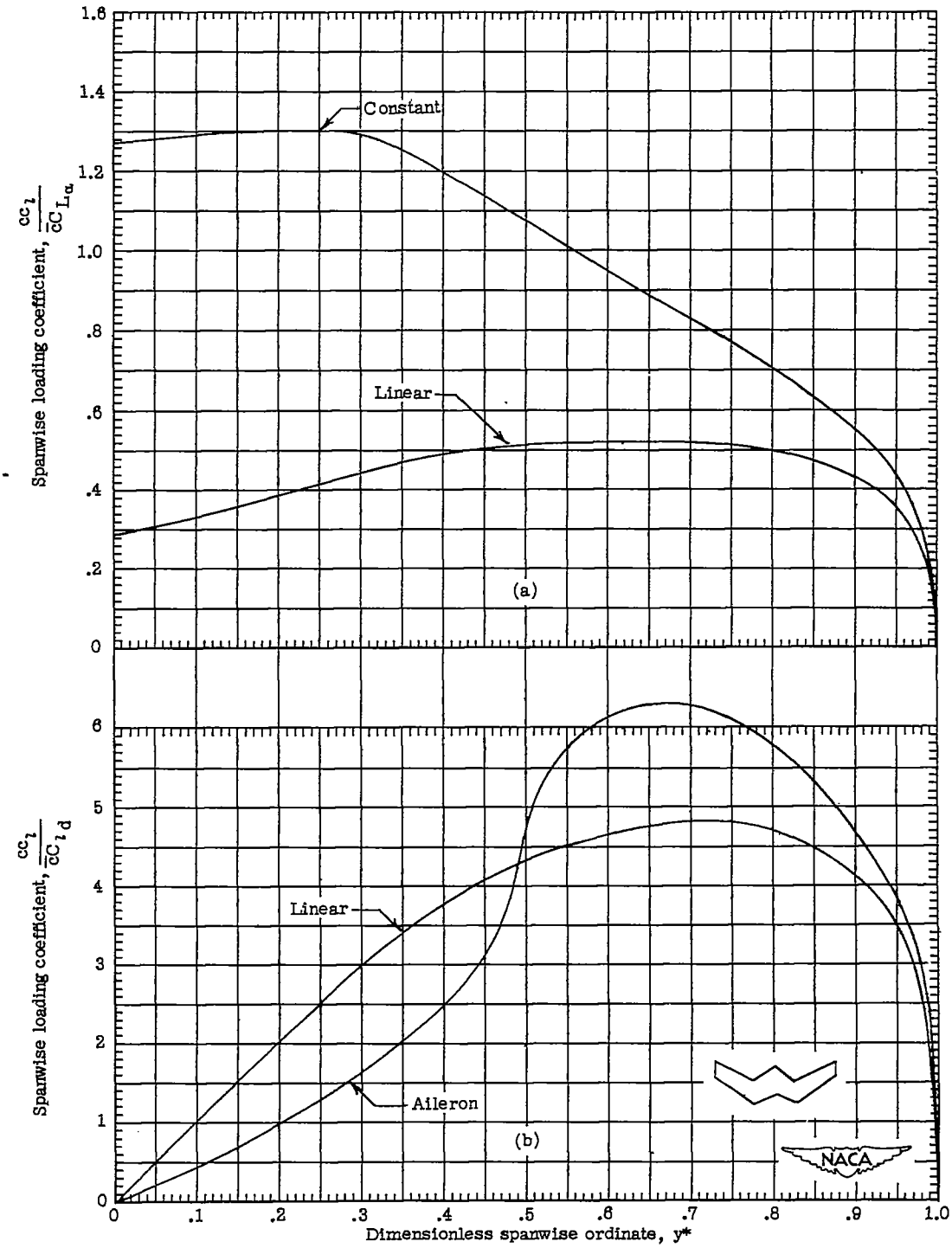

(a) Symmetrical lift distributions.

(b) Antisymmetrical lift distributions.

Figure 15.- Spanwise lift distributions for plan form 13 (A = 6, λ = 0.5, $\Lambda = \pm 30^\circ$, W wing, $y_B^* = 0.3$).

[redacted]

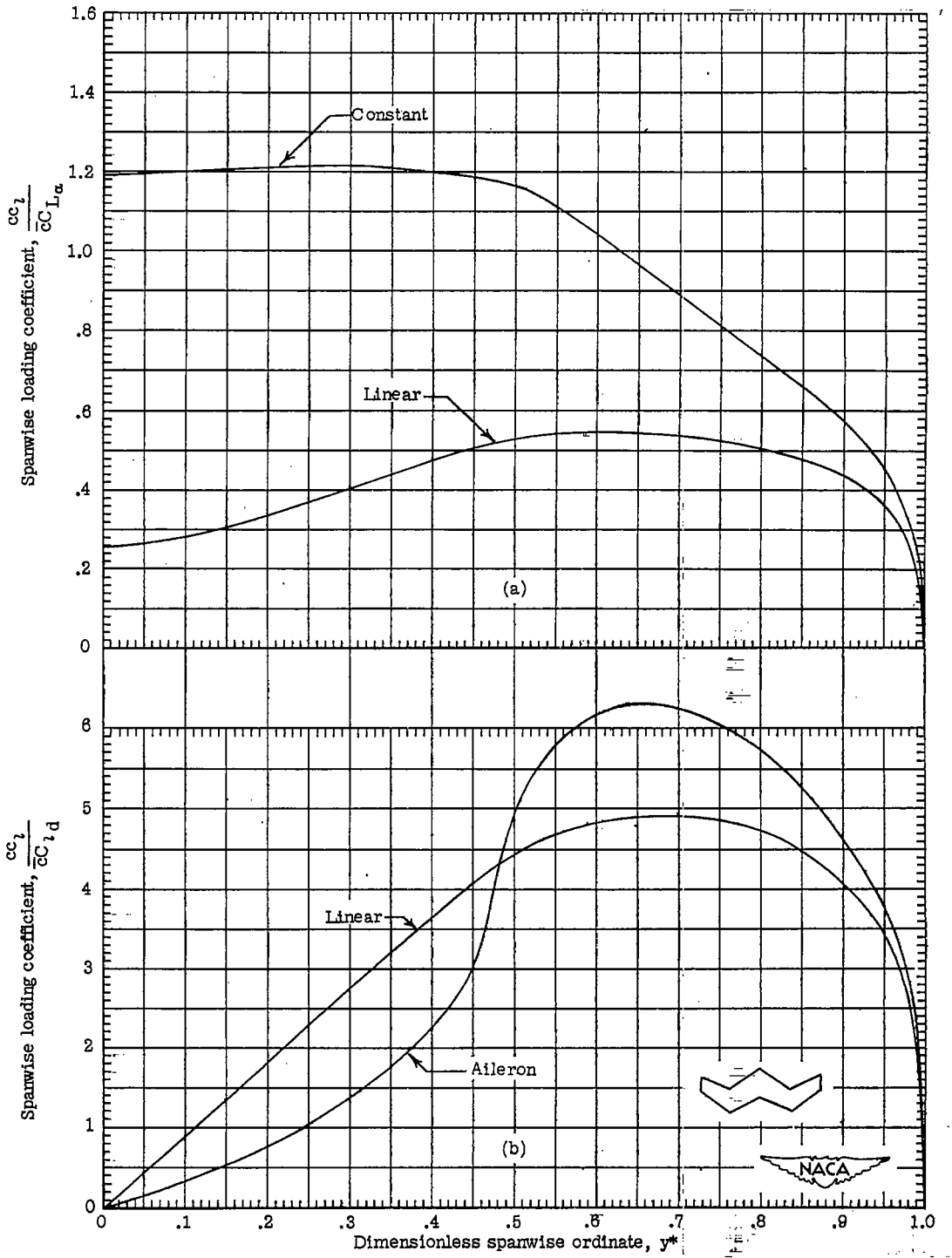

(a) Symmetrical lift distributions.

(b) Antisymmetrical lift distributions.

Figure 16.- Spanwise lift distributions for plan form 14 (A = 6, λ = 0.5, $\Lambda = \pm 30^\circ$, W wing, $y_B^* = 0.5$).

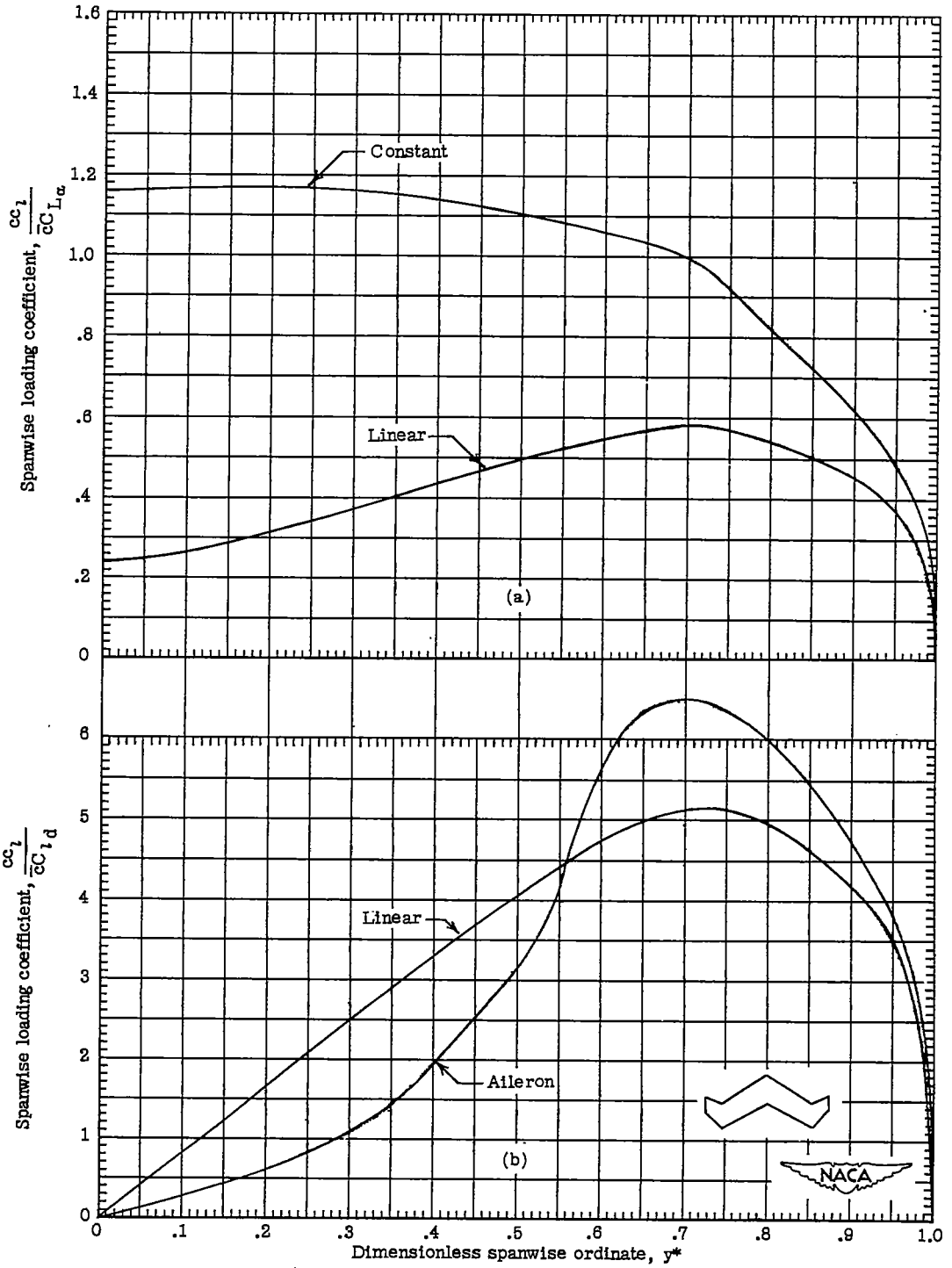

(a) Symmetrical lift distributions.

(b) Antisymmetrical lift distributions.

Figure 17.- Spanwise lift distributions for plan form 15 (A = 6, $\lambda = 0.5$, $\Lambda = \pm 30^\circ$, W wing, $y_B^* = 0.7$).

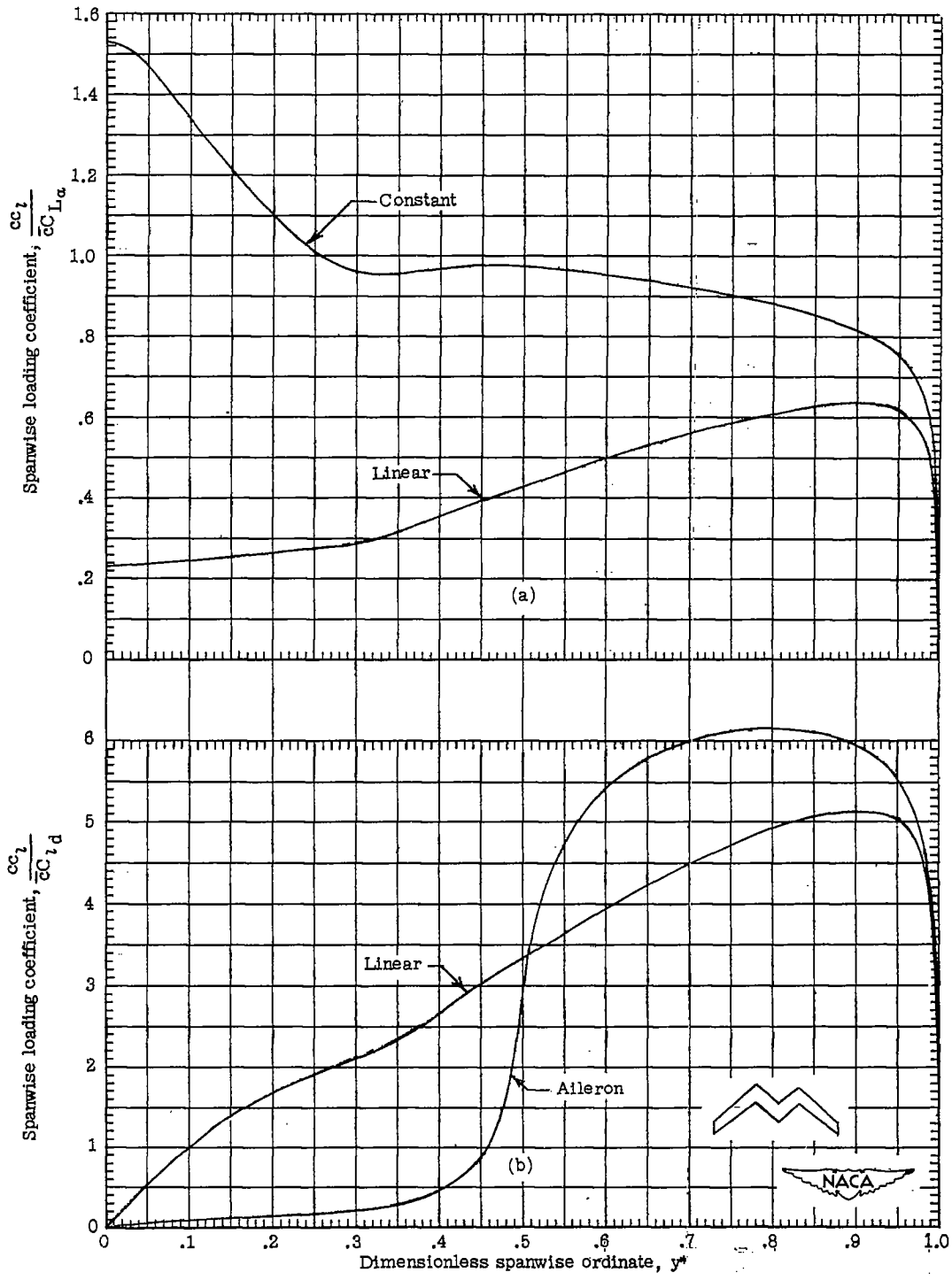

(a) Symmetrical lift distributions.

(b) Antisymmetrical lift distributions.

Figure 18.- Spanwise lift distributions for plan form 16 (A = 12, λ = 0.5, Λ = ±45°, M wing, y_B^* = 0.3).

[redacted]

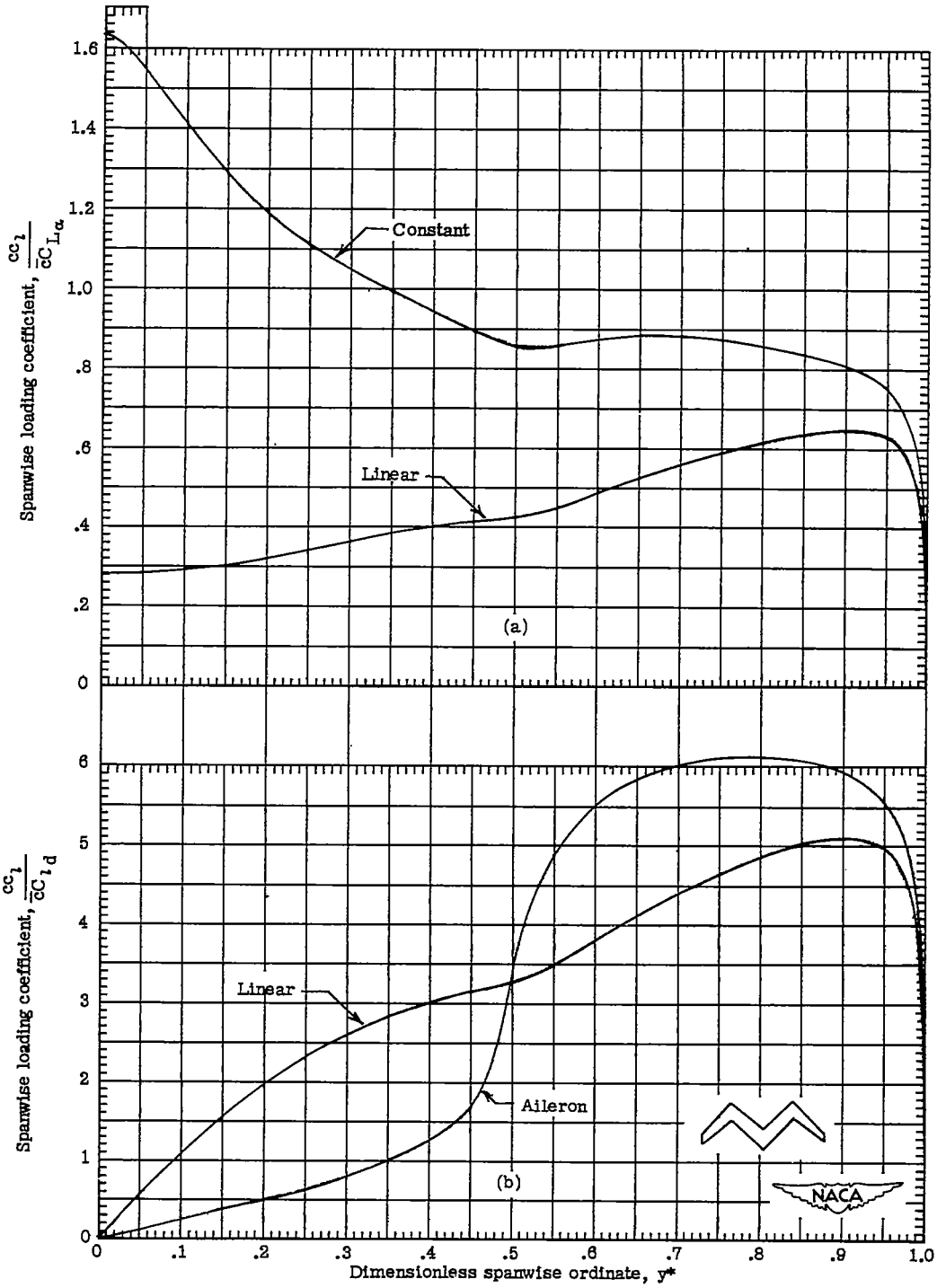

(a) Symmetrical lift distributions.

(b) Antisymmetrical lift distributions.

Figure 19.- Spanwise lift distributions for plan form 17 (A = 12, λ = 0.5, Λ = $\pm 45^\circ$, M wing, y_B^* = 0.5).

[redacted]

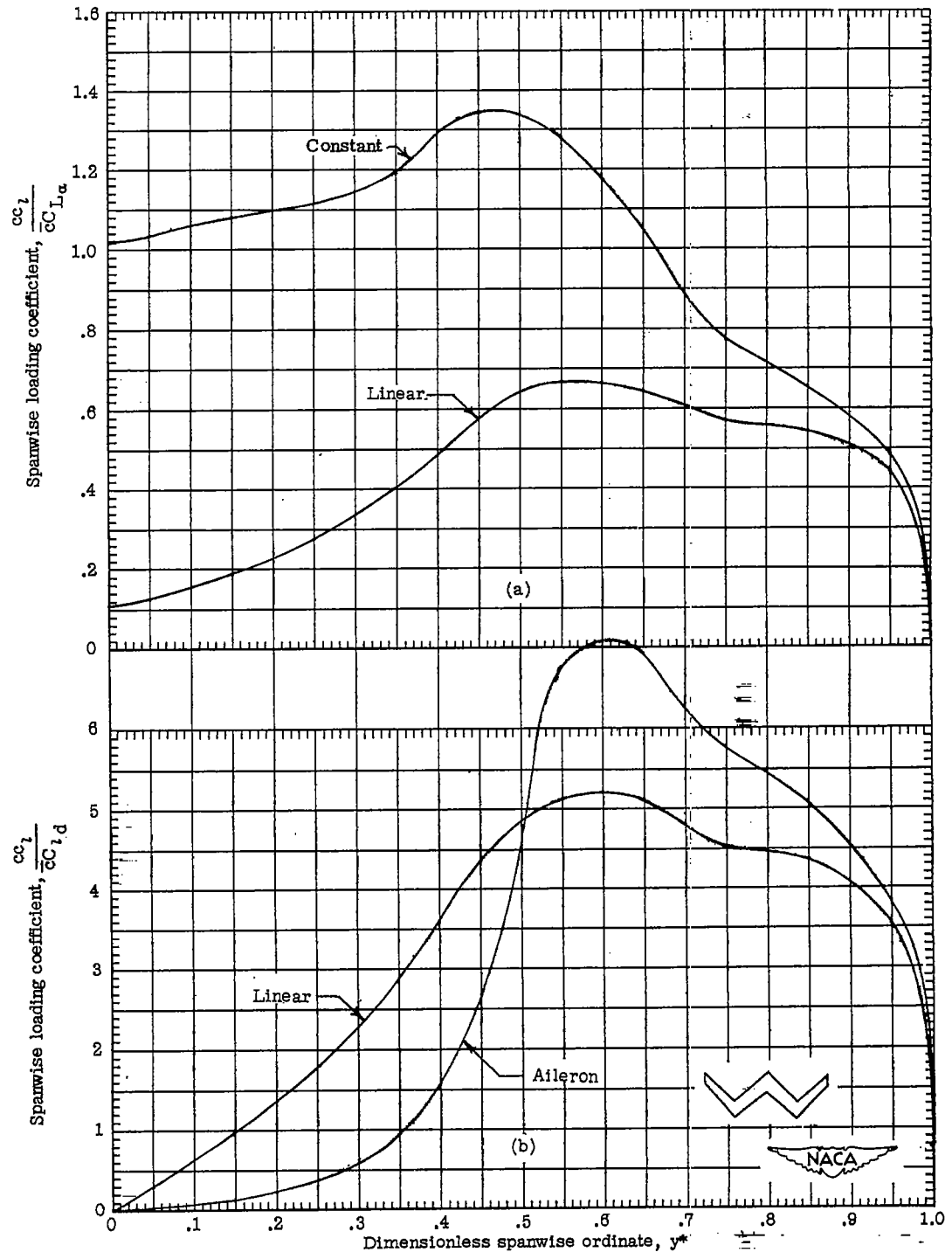

(a) Symmetrical lift distributions.

(b) Antisymmetrical lift distributions.

Figure 20.- Spanwise lift distributions for plan form 18 (A = 12, λ = 0.5, Λ = $\pm 45^\circ$, W wing, y_B^* = 0.5).

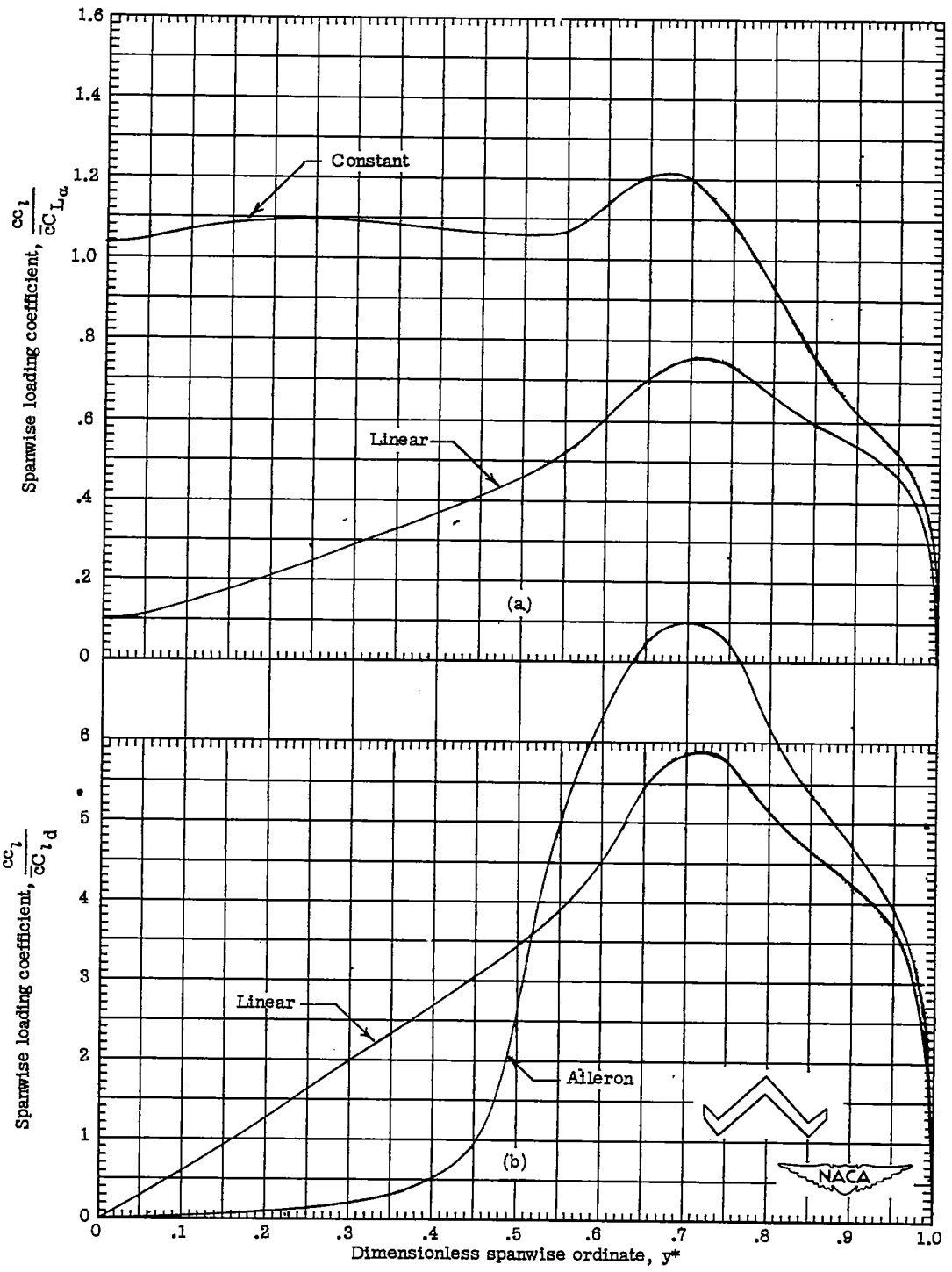

(a) Symmetrical lift distributions.

(b) Antisymmetrical lift distributions.

Figure 21.- Spanwise lift distributions for plan form 19 ($A = 12$, $\lambda = 0.5$, $\Lambda = \pm 45^\circ$, W wing, $y_B^* = 0.7$).

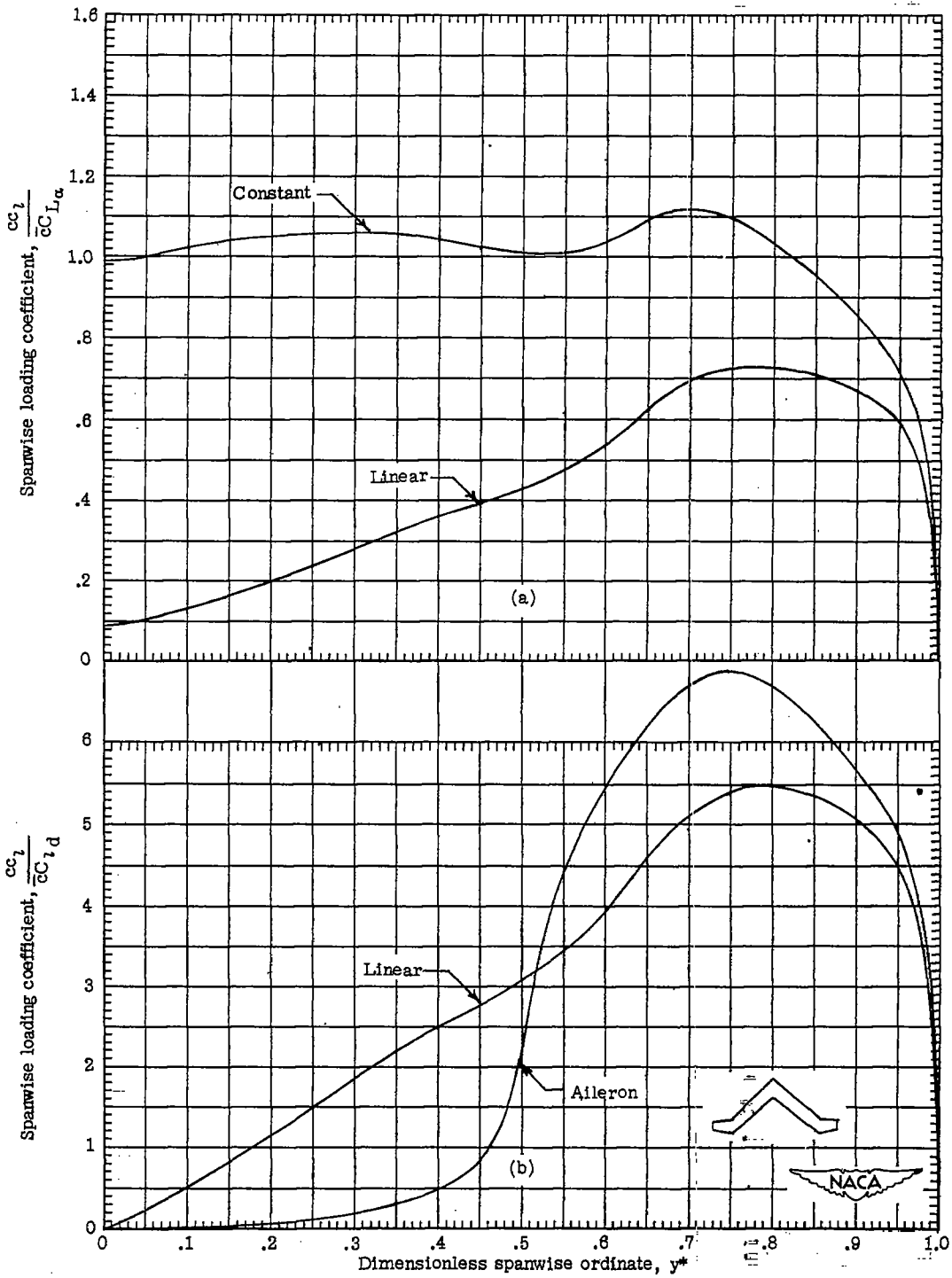

(a) Symmetrical lift distributions.

(b) Antisymmetrical lift distributions.

Figure 22.- Spanwise lift distributions for plan form 20 (A = 12, λ = 0.5, Λ_i = 45°, Λ wing, y_B^* = 0.7).

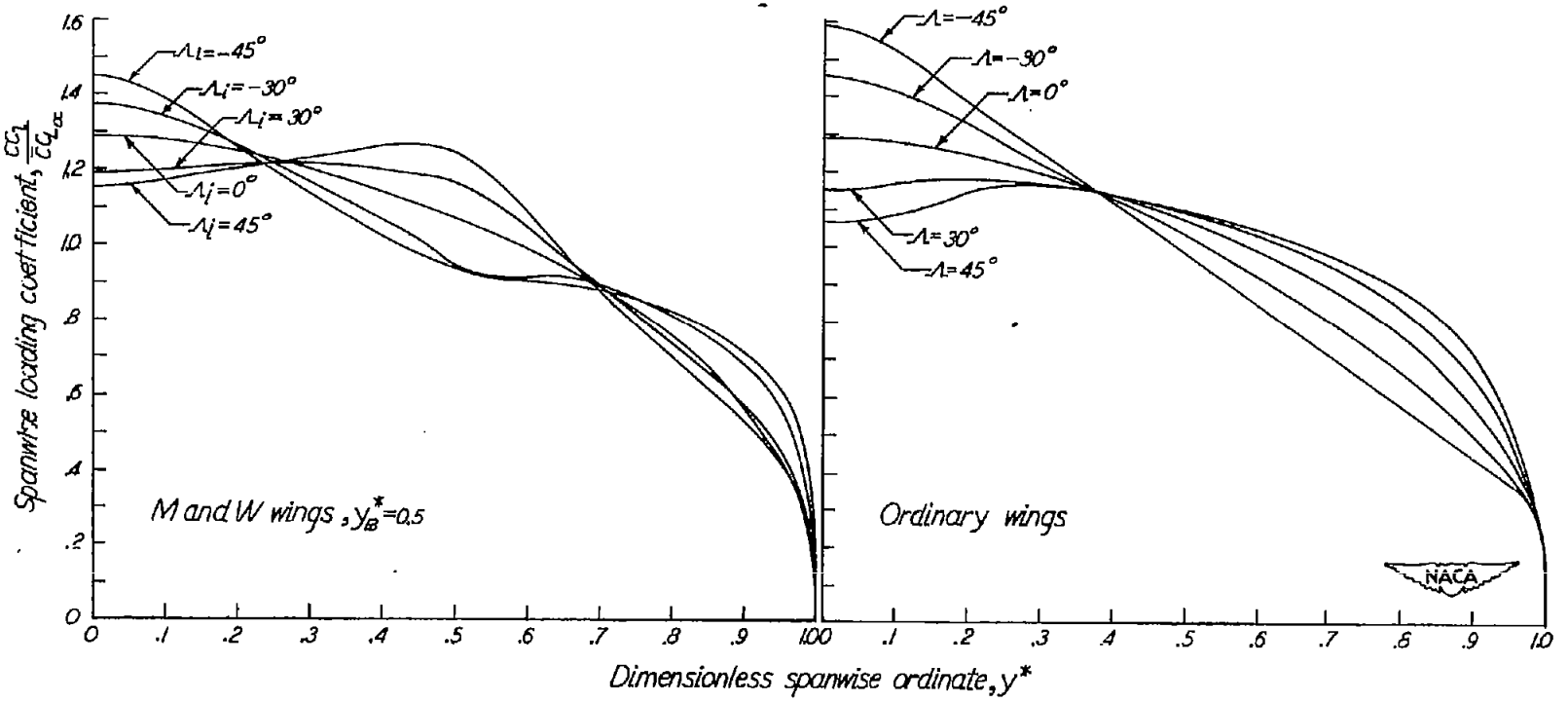

(a) $A=6$.

Figure 23.- Effect of angle of sweep on the lift distributions of M, W, and ordinary swept wings of taper ratio 0.5.

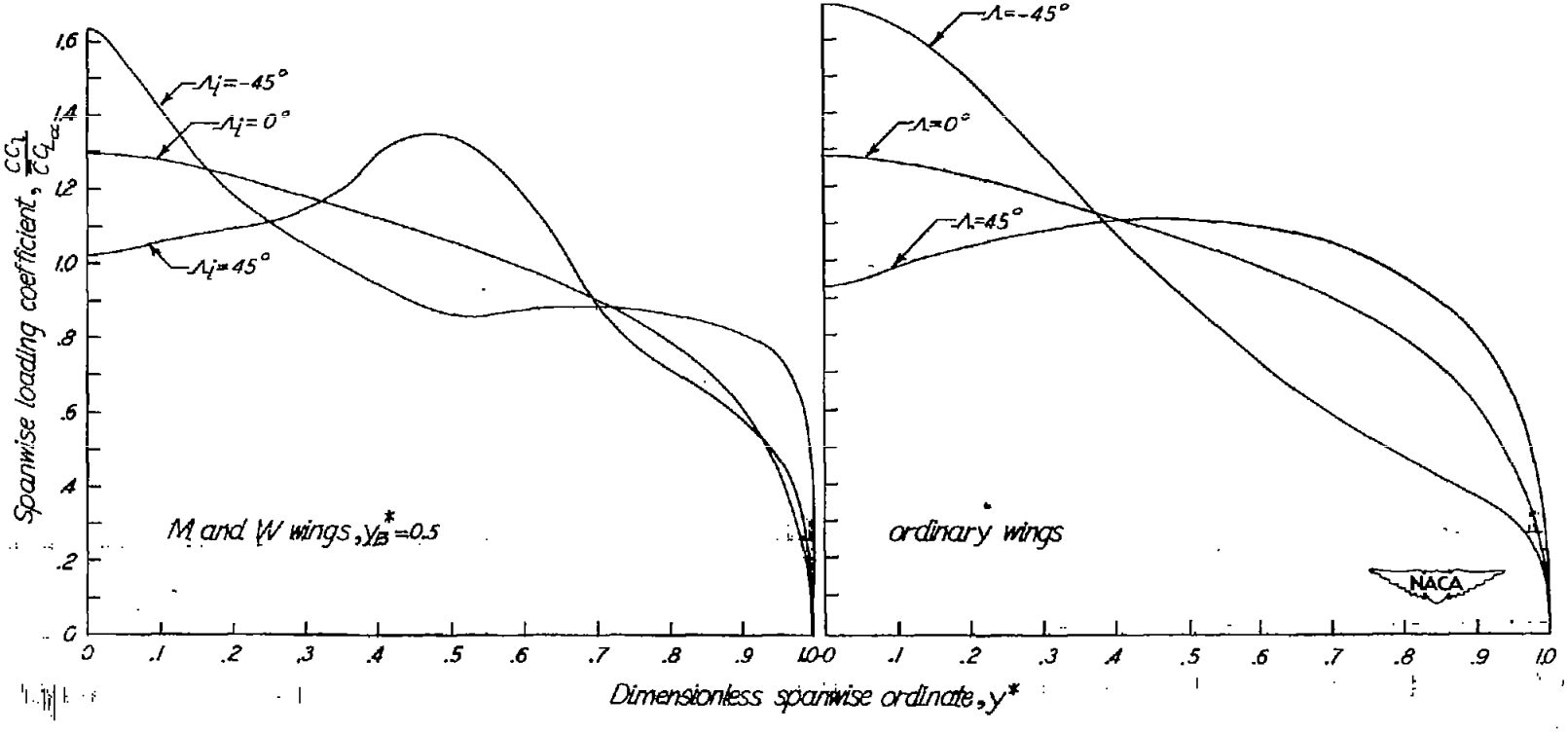

(b) A=12.

Figure 23.- Concluded.

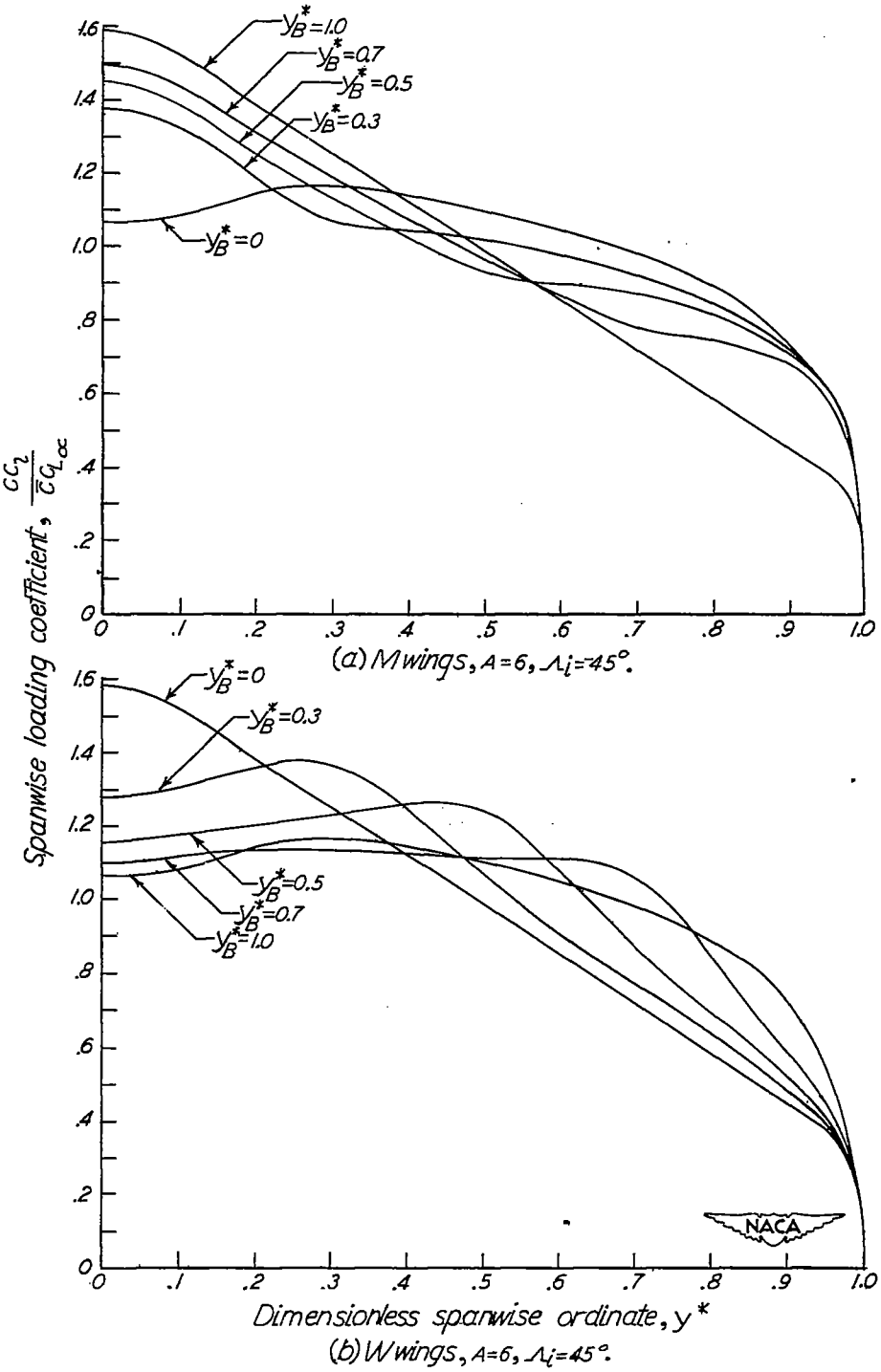

Figure 24.- Effect of position of discontinuity in sweep angle on the lift distribution of M and W wings of taper ratio 0.5.

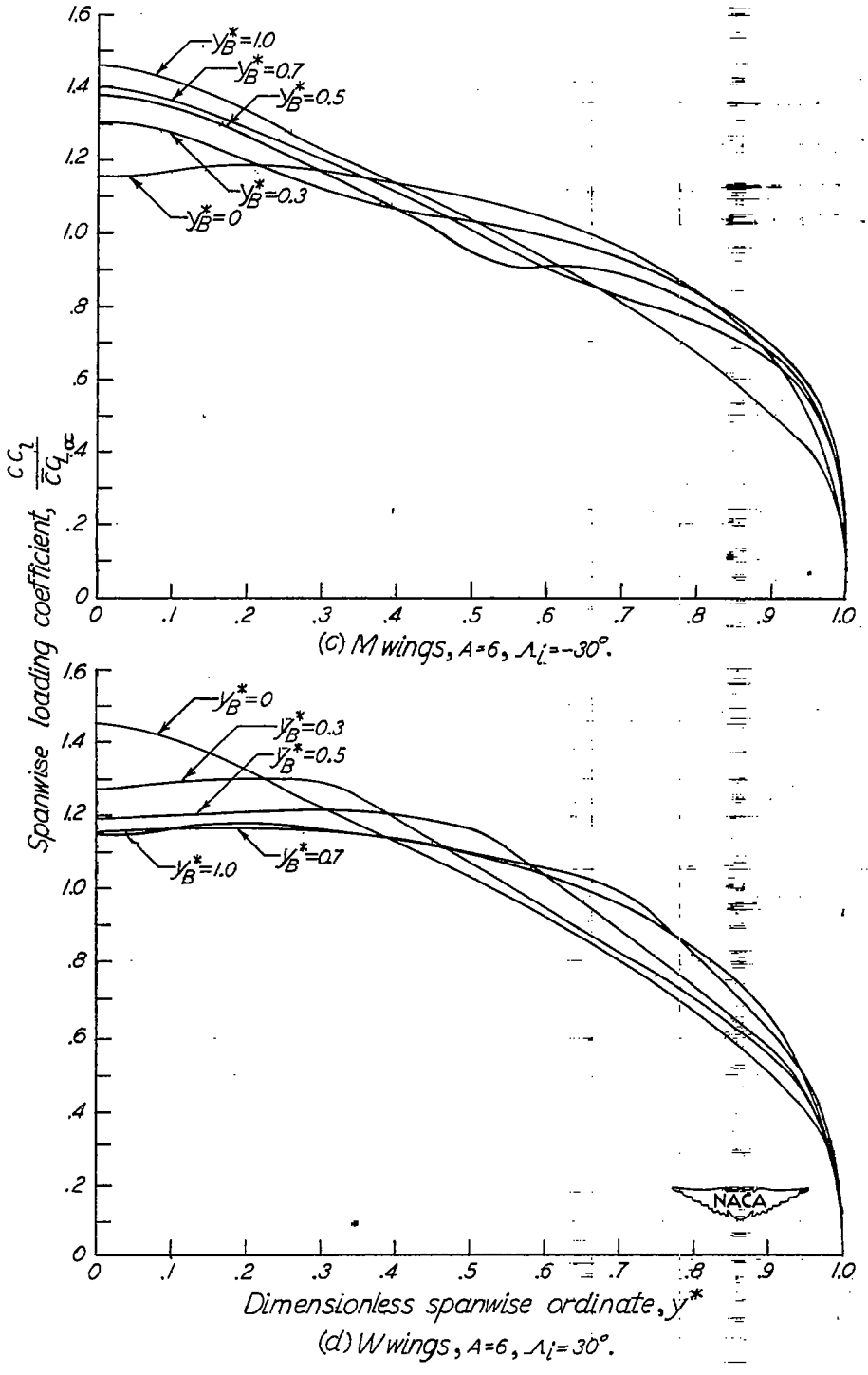

Figure 24.- Continued.

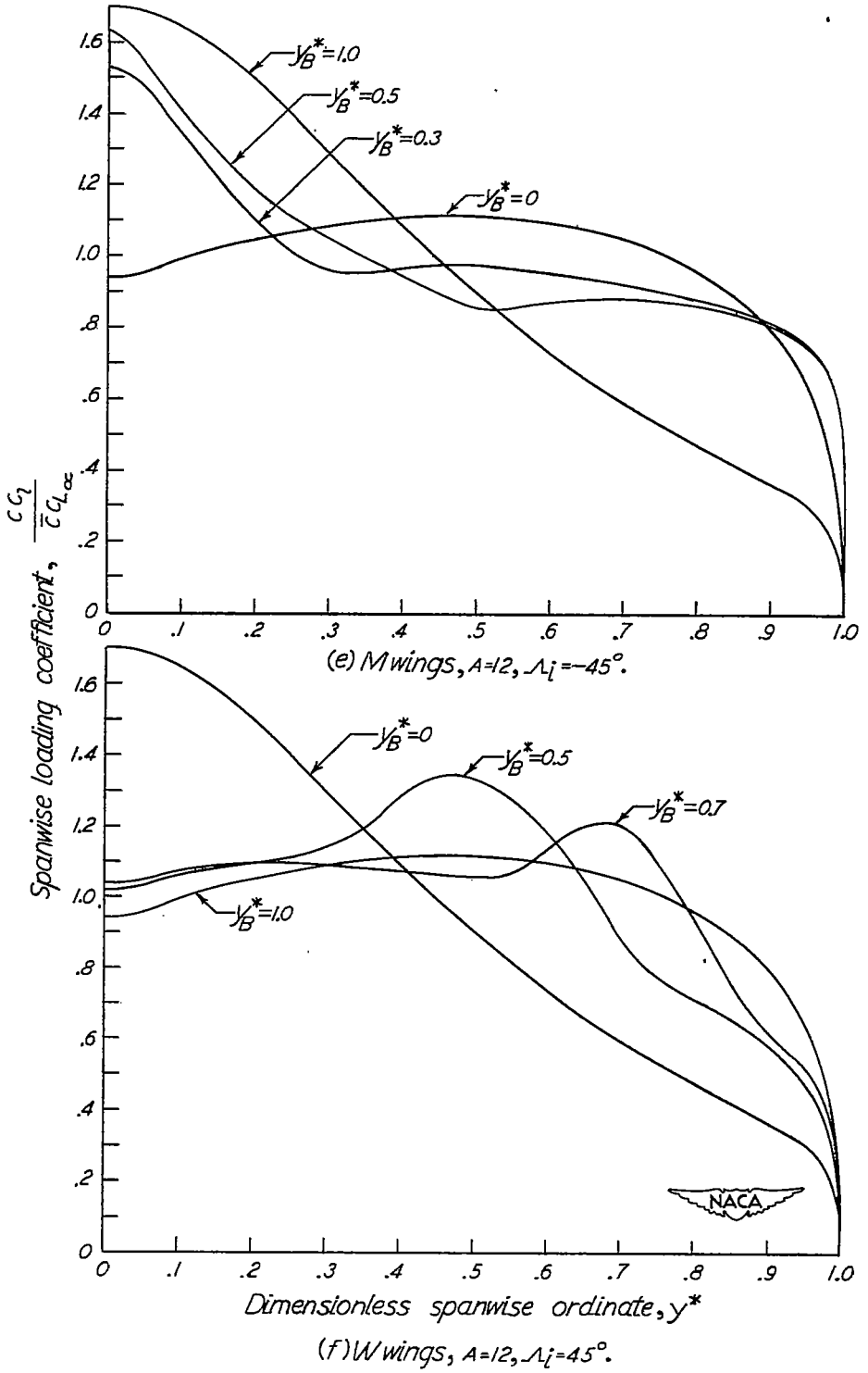

Figure 24.- Concluded.

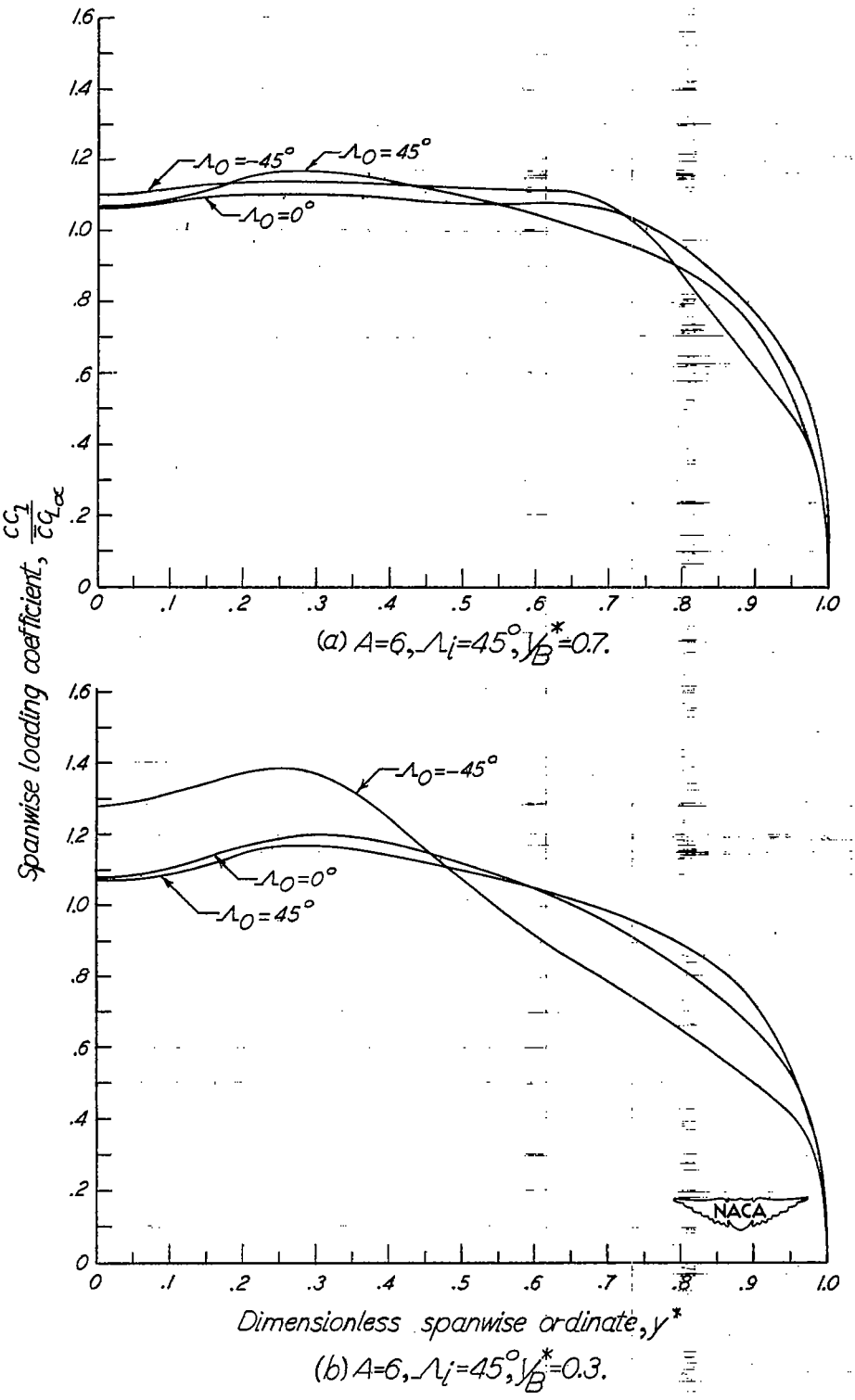

Figure 25.- Effect of sweep of the outer portion of the wing on the lift distribution of wings with taper ratio 0.5.

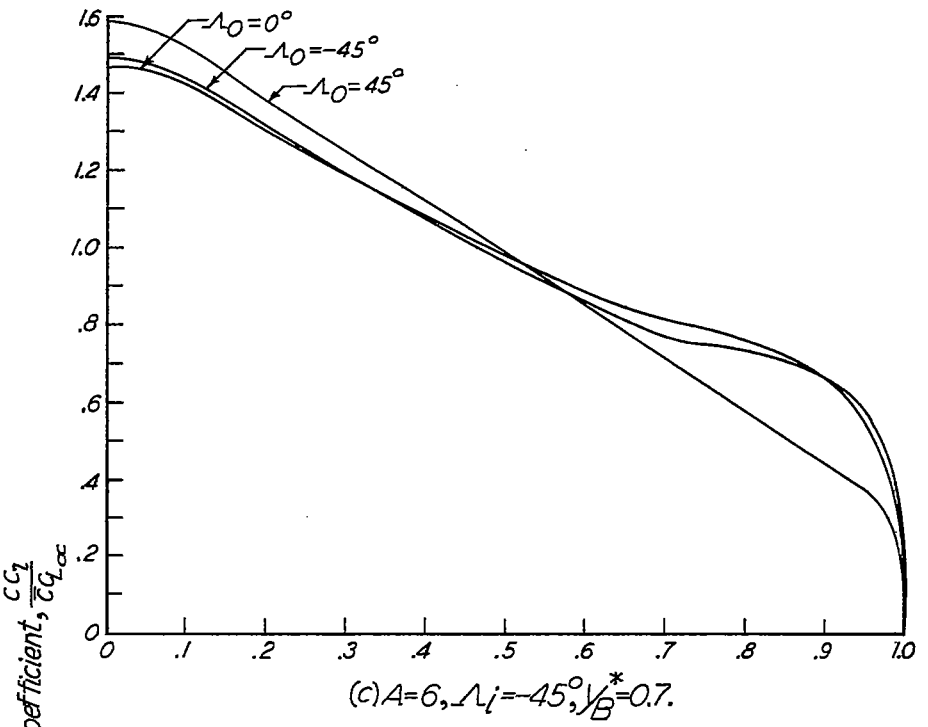

(c) $A=6$, $\Lambda_i=-45°$, $y_B^*=0.7$.

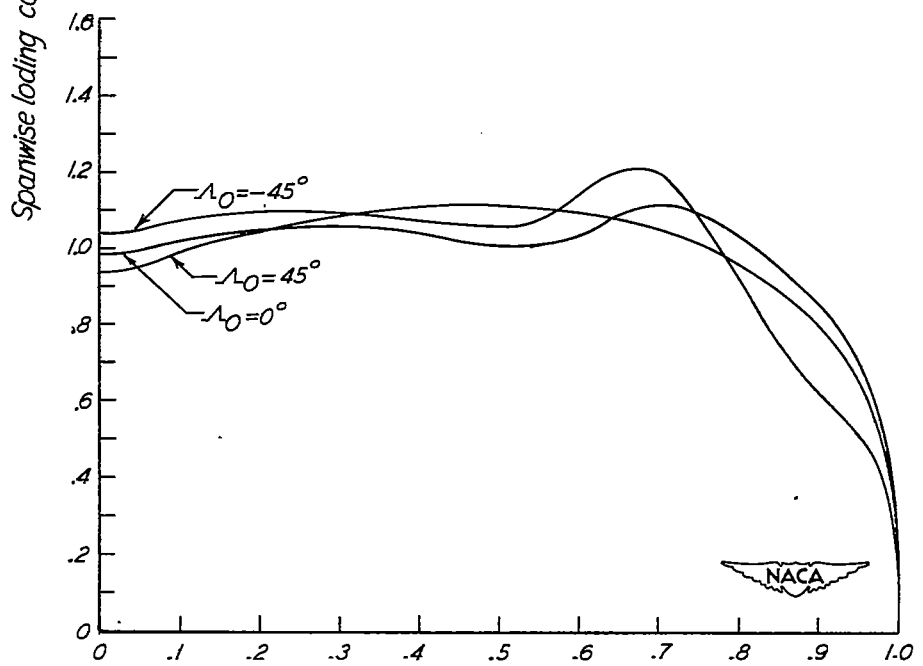

(d) $A=12$, $\Lambda_i=45°$, $y_B^*=0.7$.

Figure 25.- Concluded.

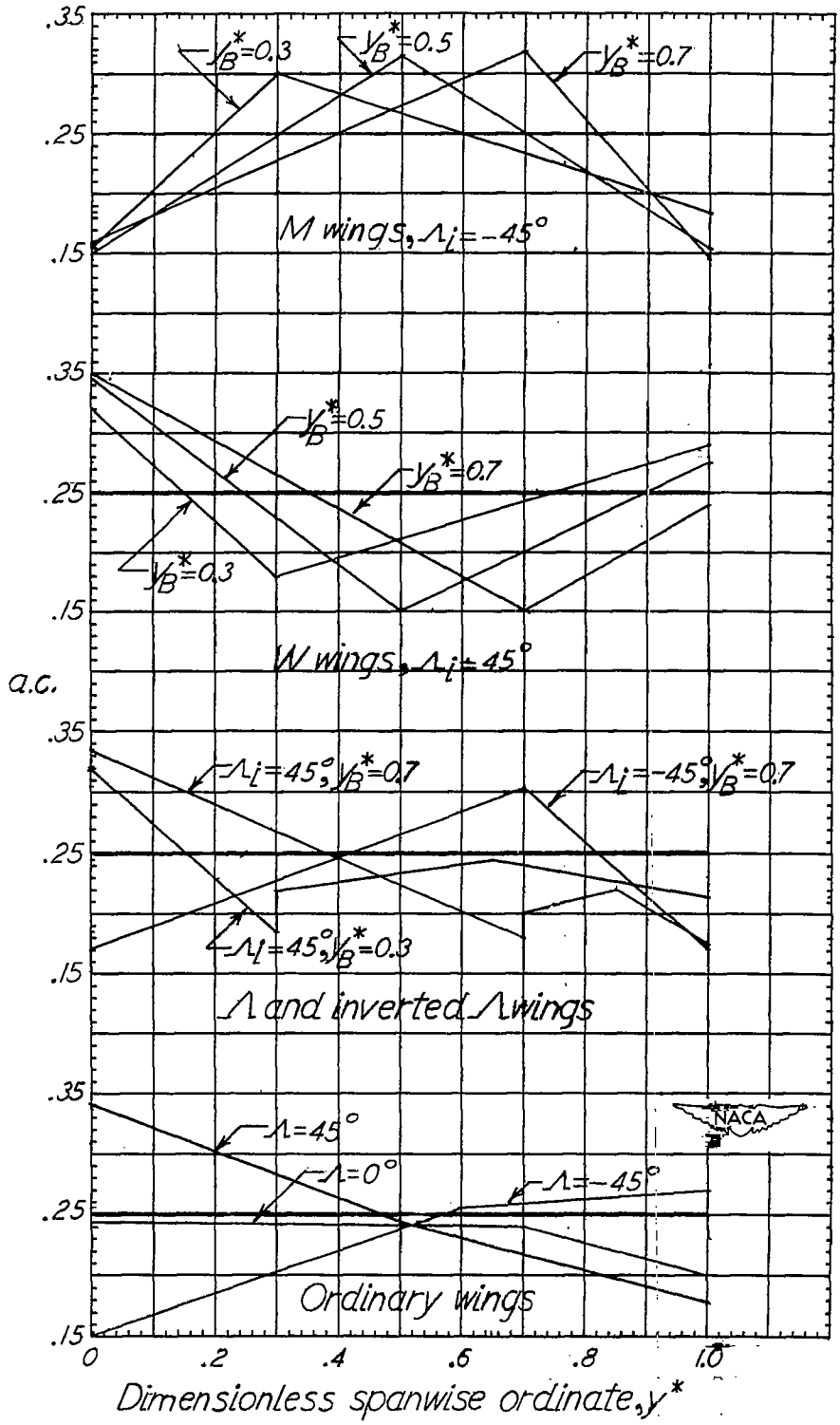

Figure 26.- Assumed local aerodynamic centers for wings of aspect ratio 6, taper ratio 0.5.

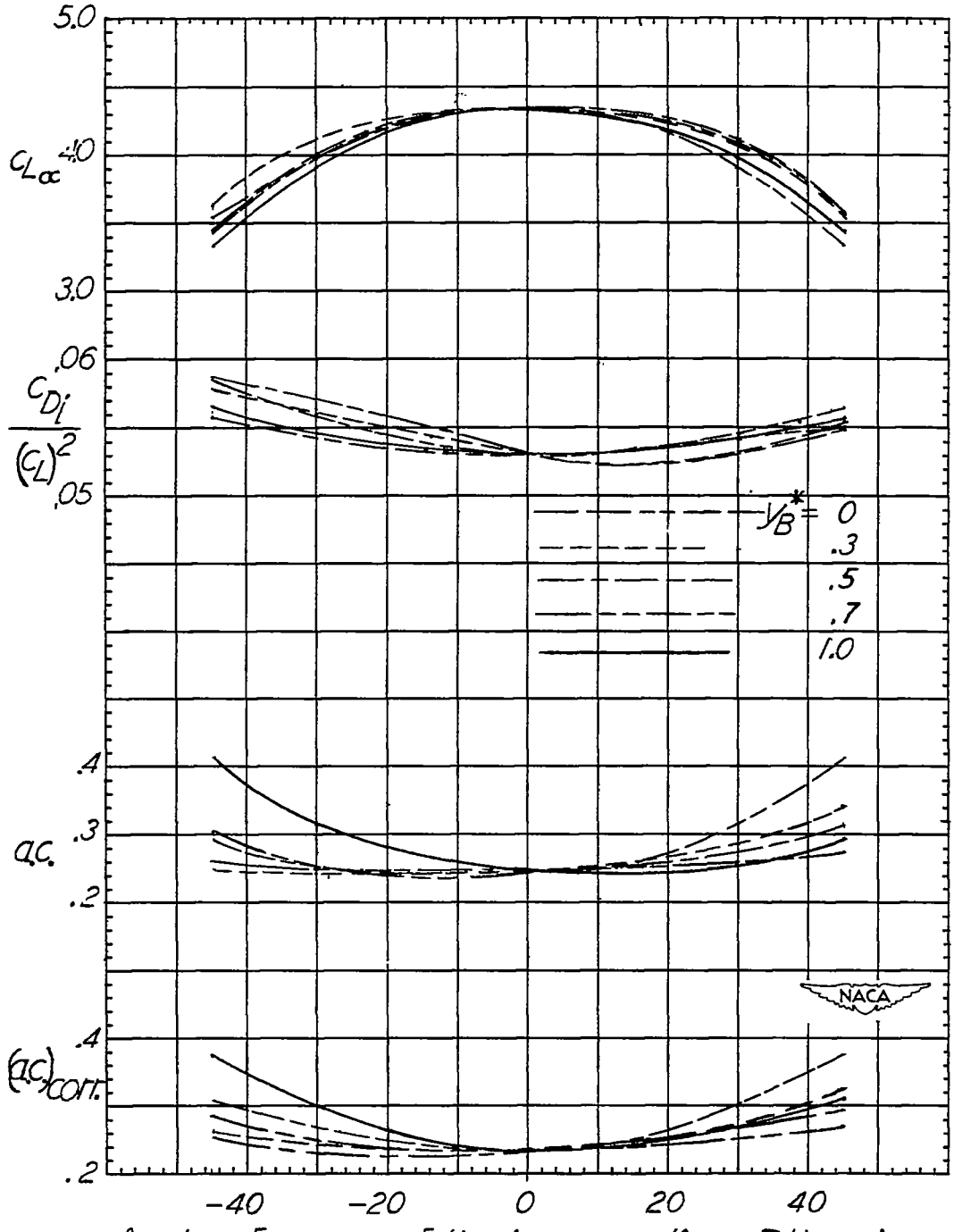

(a) A=6.

Figure 27.- Aerodynamic characteristics of M and W wings of taper ratio 0.5.

[redacted]

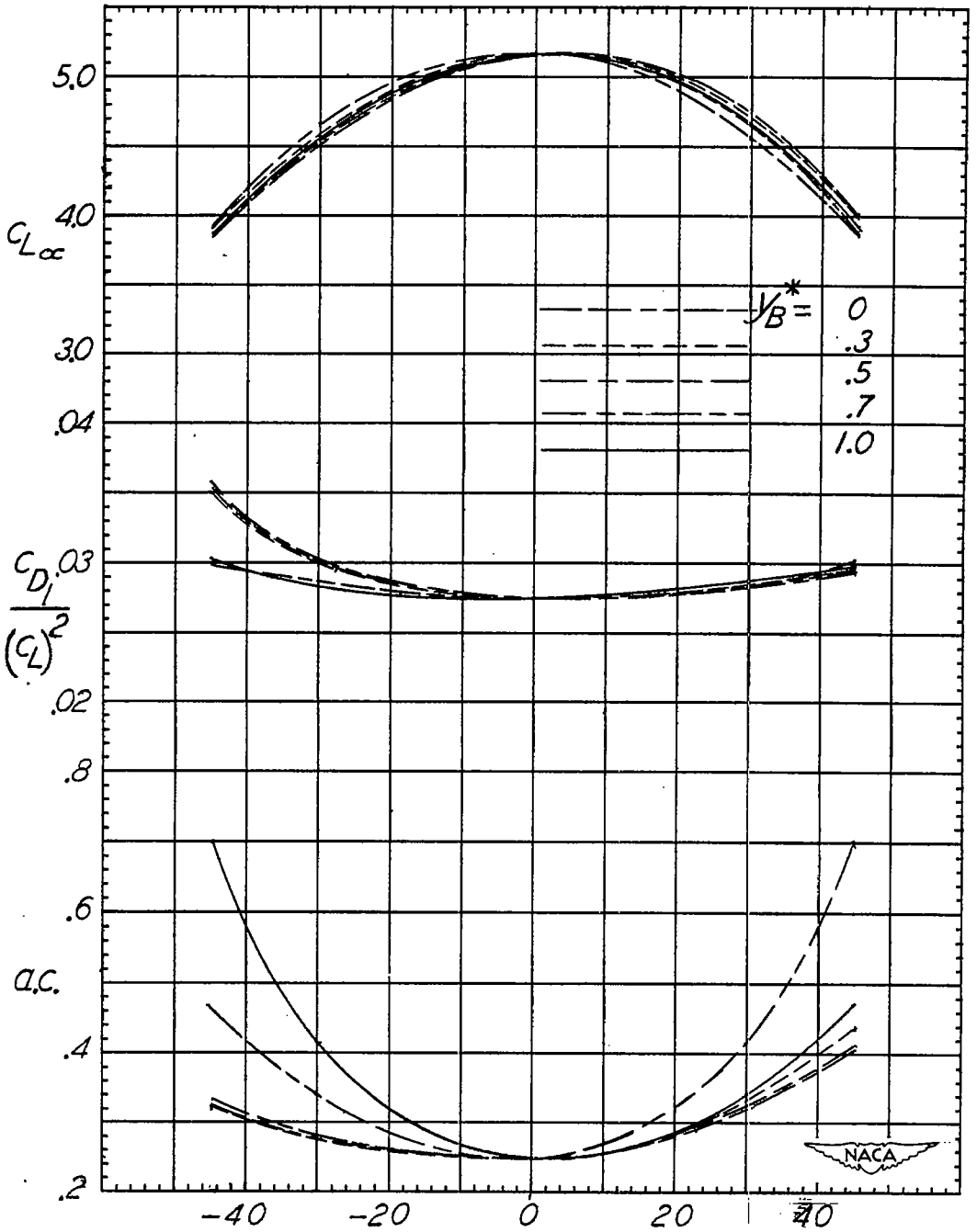

(b) A = 12.

Figure 27.- Concluded.

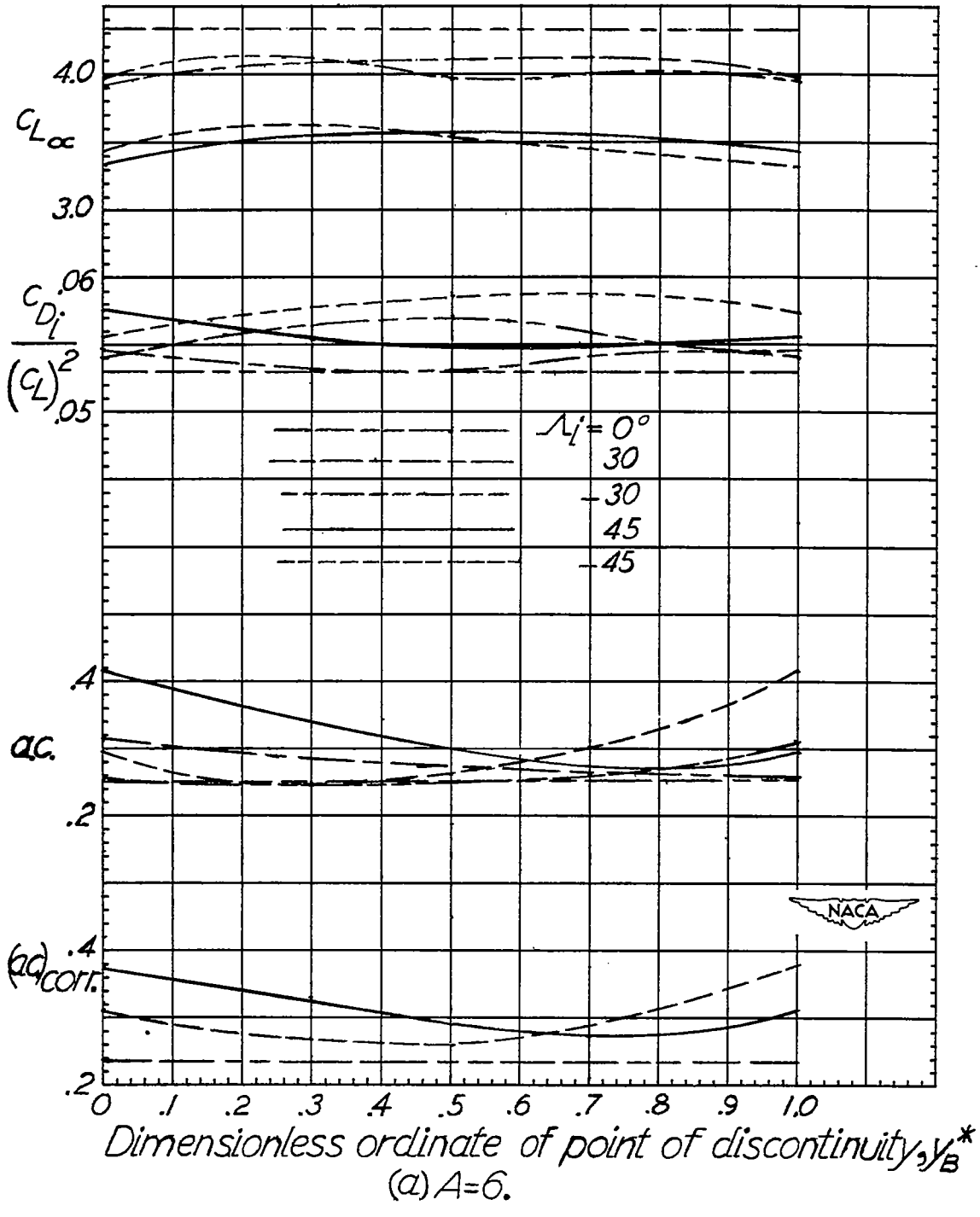

Figure 28.- Effect of location of the spanwise discontinuity in the angle of sweep on the aerodynamic characteristics of M and W wings, taper ratio 0.5.

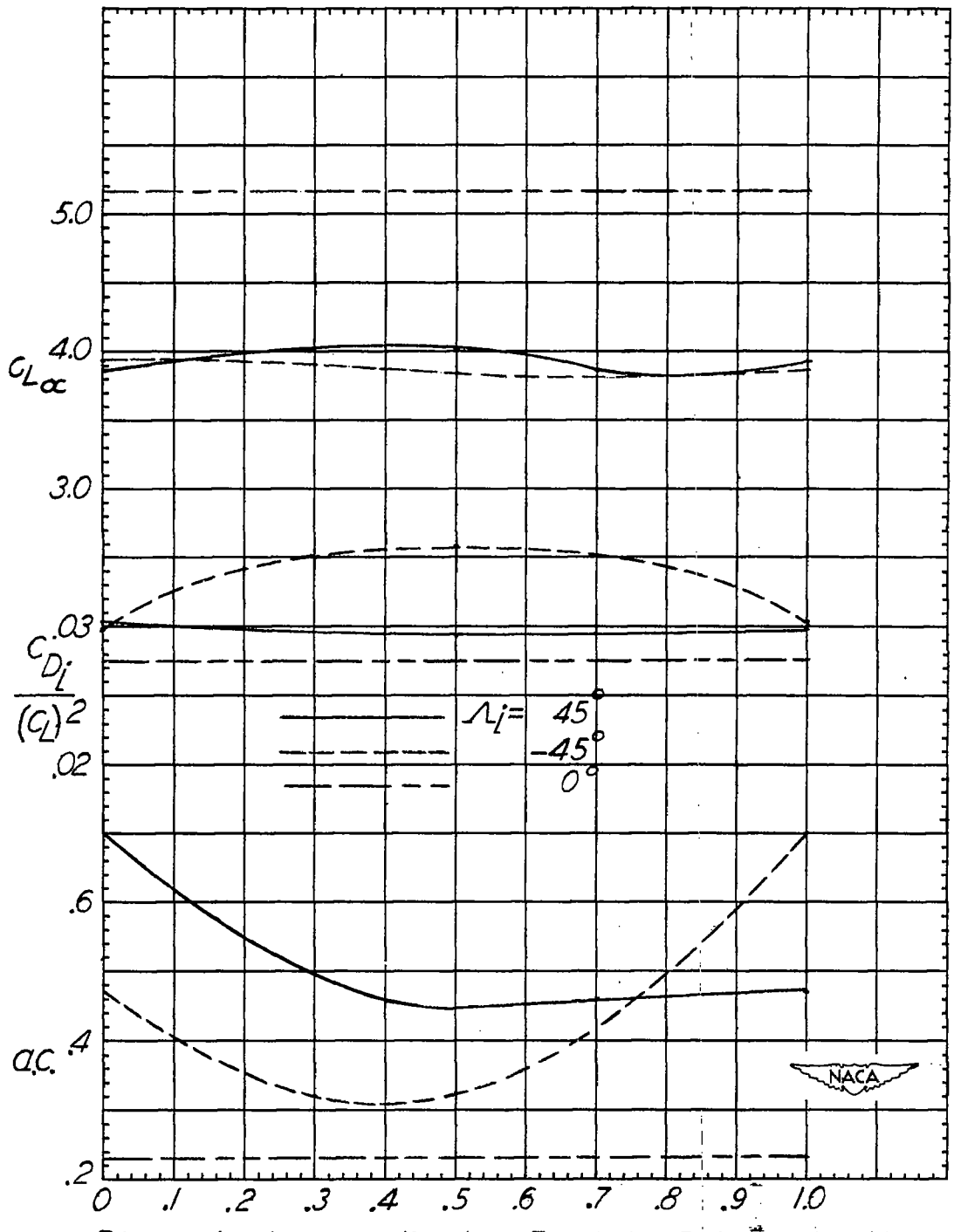

Figure 28 - Concluded.

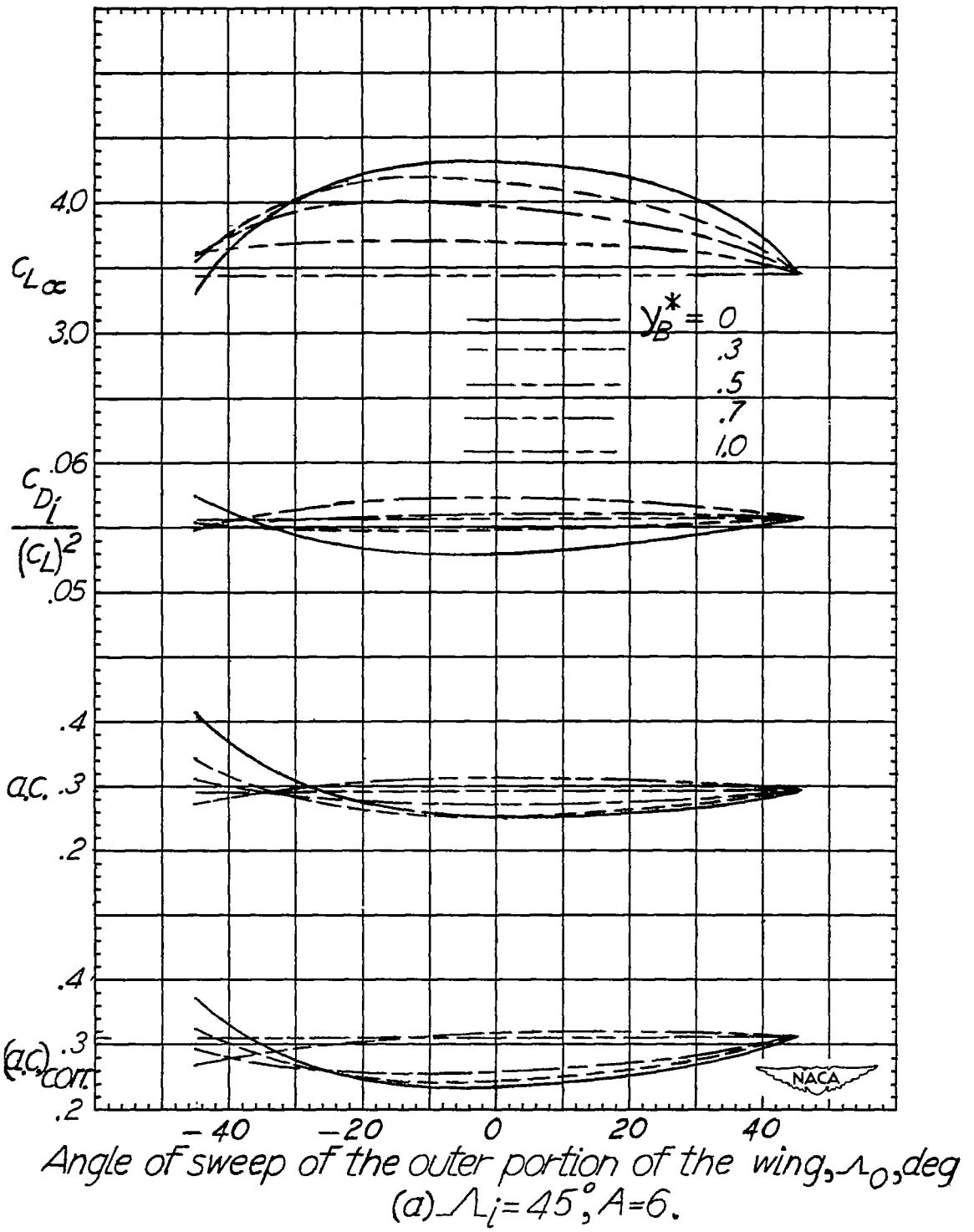

Figure 29.- Effect of sweep of outer portion on aerodynamic characteristics.

[redacted]

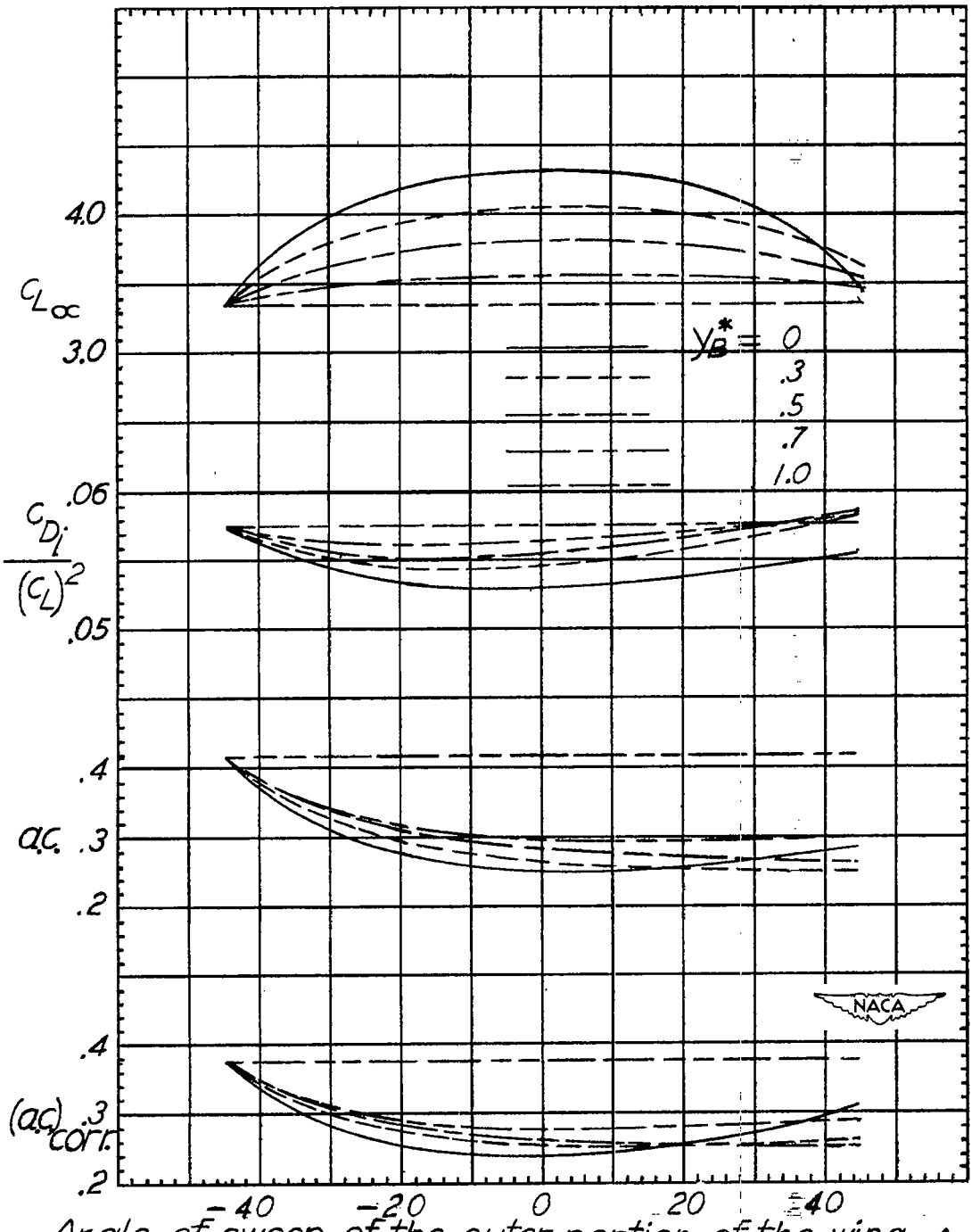

(b) $\Lambda_i = -45°$, $A = 6$.

Figure 29.- Continued.

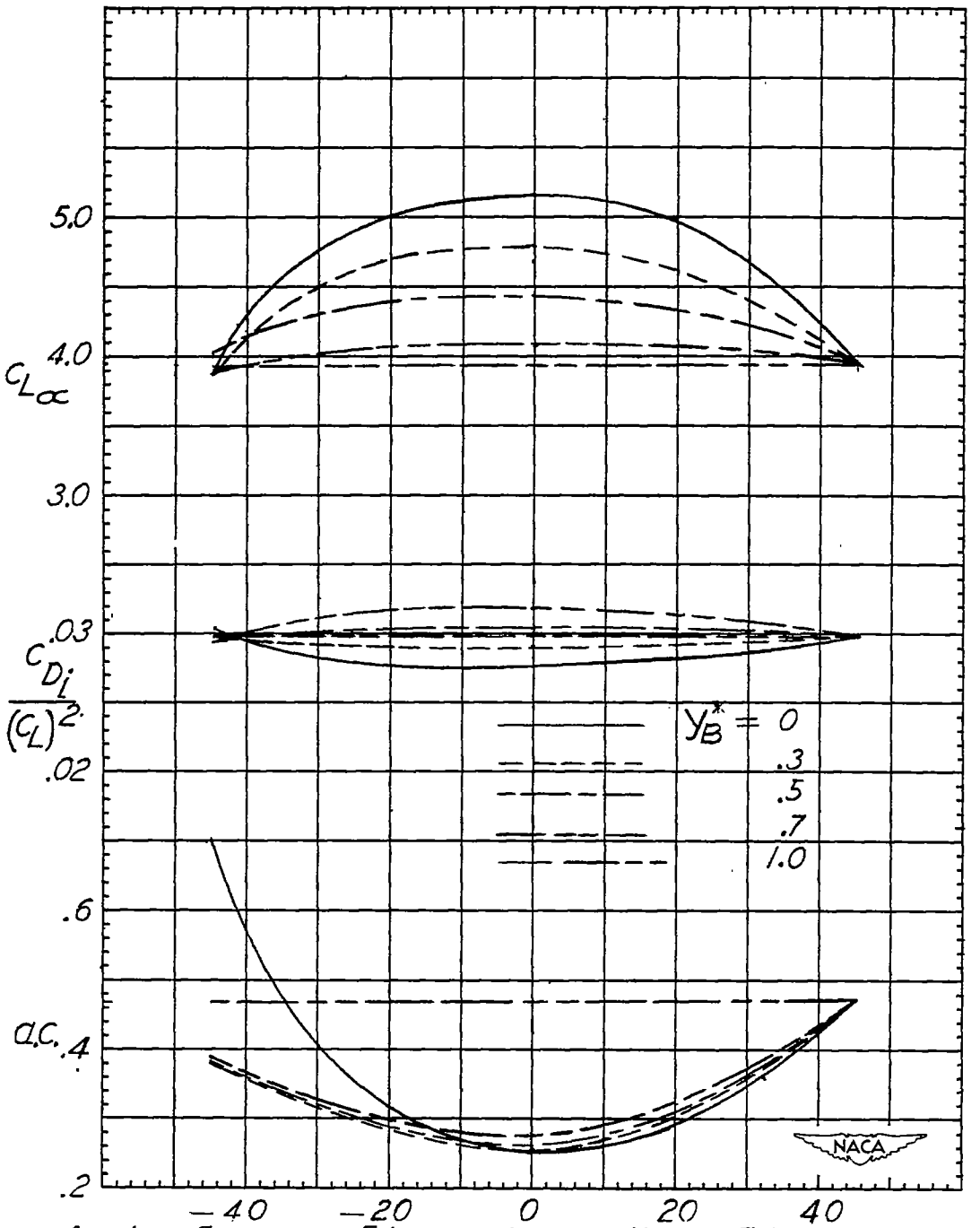

(c) $\Lambda_i = 45°$, $A = 12$.

Figure 29.- Continued.

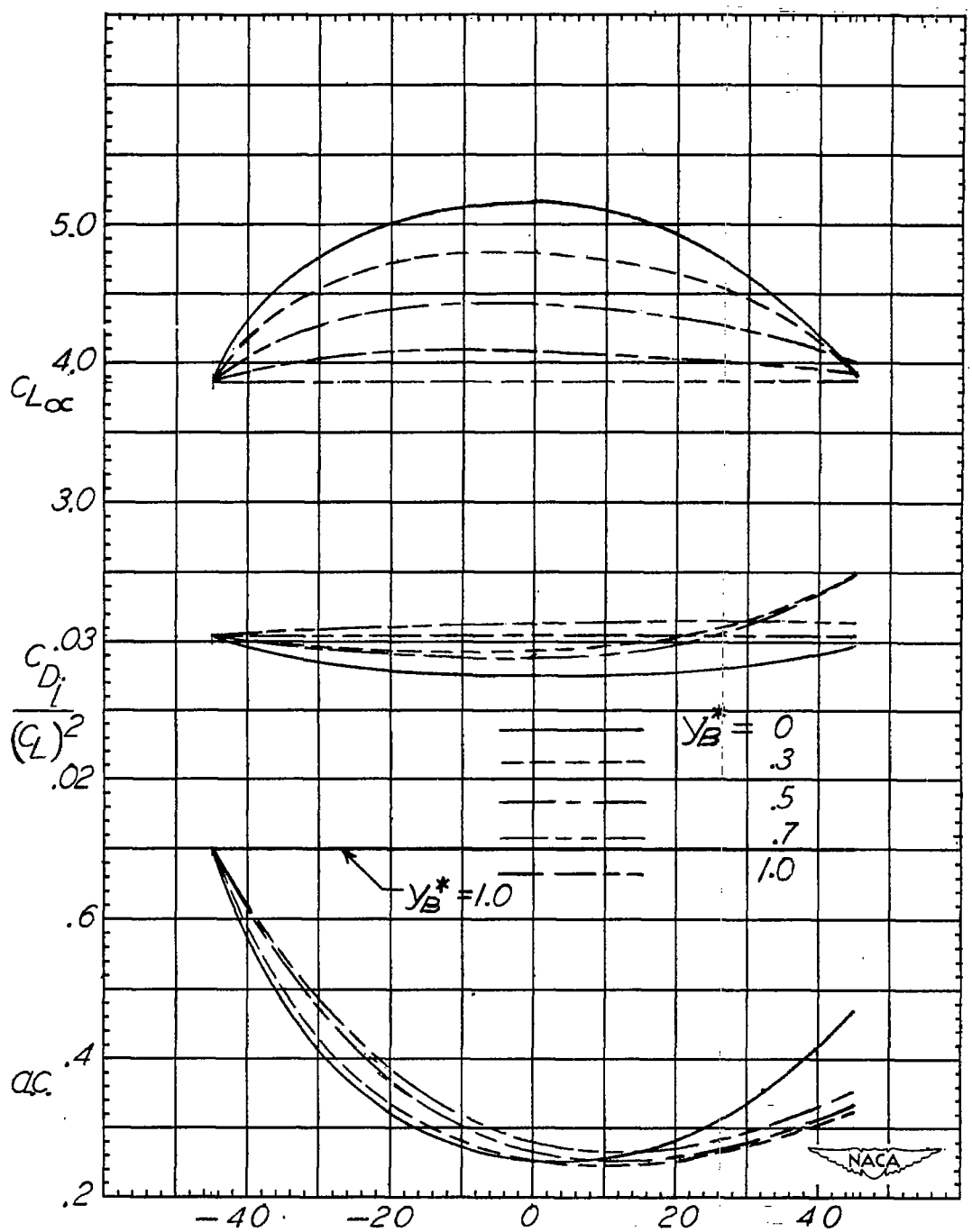

(d) $\Lambda_i = -45°$, $A = 12$.

Figure 29.- Concluded.

NACA-Langley - 8-30-51 - 385